Hepatocyte-specific suppression of ANGPTL4 improves obesity-associated diabetes and mitigates atherosclerosis in mice

Abhishek K. Singh,[1,2] Balkrishna Chaube,[1,2] Xinbo Zhang,[1,2] Jonathan Sun,[1,2] Kathryn M. Citrin,[1,2,3] Alberto Canfrán-Duque,[1,2] Binod Aryal,[1,2] Noemi Rotllan,[1,2] Luis Varela,[2] Richard G. Lee,[4] Tamas L. Horvath,[2] Nathan L. Price,[1,2] Yajaira Suárez,[1,2,5] and Carlos Fernández-Hernando[1,2,5]

[1]Vascular Biology and Therapeutics Program, [2]Integrative Cell Signaling and Neurobiology of Metabolism Program, Department of Comparative Medicine, and [3]Department of Cellular and Molecular Physiology, Yale University School of Medicine, New Haven, Connecticut, USA. [4]Cardiovascular Group, Antisense Drug Discovery, Ionis Pharmaceuticals, Carlsbad, California, USA. [5]Department of Pathology, Yale University School of Medicine, New Haven, Connecticut, USA.

Hepatic uptake and biosynthesis of fatty acids (FAs), as well as the partitioning of FAs into oxidative, storage, and secretory pathways, are tightly regulated processes. Dysregulation of one or more of these processes can promote excess hepatic lipid accumulation, ultimately leading to systemic metabolic dysfunction. Angiopoietin-like-4 (ANGPTL4) is a secretory protein that inhibits lipoprotein lipase (LPL) and modulates triacylglycerol (TAG) homeostasis. To understand the role of ANGPTL4 in liver lipid metabolism under normal and high-fat–fed conditions, we generated hepatocyte-specific *Angptl4* mutant mice (*Hmut*). Using metabolic turnover studies, we demonstrate that hepatic *Angptl4* deficiency facilitates catabolism of TAG-rich lipoprotein (TRL) remnants in the liver via increased hepatic lipase (HL) activity, which results in a significant reduction in circulating TAG and cholesterol levels. Consequently, depletion of hepatocyte *Angptl4* protects against diet-induced obesity, glucose intolerance, liver steatosis, and atherogenesis. Mechanistically, we demonstrate that loss of *Angptl4* in hepatocytes promotes FA uptake, which results in increased FA oxidation, ROS production, and AMPK activation. Finally, we demonstrate the utility of a targeted pharmacologic therapy that specifically inhibits *Angptl4* gene expression in the liver and protects against diet-induced obesity, dyslipidemia, glucose intolerance, and liver damage, which likely occur via increased HL activity. Notably, this inhibition strategy does not cause any of the deleterious effects previously observed with neutralizing antibodies.

Introduction

The liver is a central metabolic organ that is essential for regulating systemic glucose and lipid homeostasis (1, 2). Lipid homeostasis is maintained by the liver via a regulated balance between lipid acquisition (fatty acid [FA] uptake and biosynthesis) and removal (FA oxidation [FAO] and VLDL secretion) (3–5). Dysregulation in these critical processes leads to the accumulation of excess triacylglycerol (TAG) in hepatocytes, resulting in the development of nonalcoholic fatty liver disease (NAFLD) and associated disorders, such as hepatic insulin resistance (IR), type 2 diabetes (T2D), and atherosclerosis (5–10). The key pathological feature of NAFLD is the accumulation of intrahepatic TAG, owing to increased flux of free FA (FFA) derived from lipolysis in adipose tissue (AT), dietary chylomicrons, and intrahepatic de novo lipogenesis (DNL) (5, 11). Lipoprotein lipase (LPL) plays a vital role in the homeostasis of lipid metabolism at the systemic level. However, the cellular mechanisms behind the regulation of lipid homeostasis in the liver still remain unclear.

Angiopoietin-like-4 (ANGPTL4) is a multifaceted secreted protein that is highly expressed in metabolic tissues, most prominently in AT and liver (12–14). ANGPTL4 regulates many cellular and physiological functions, mainly via inhibiting LPL activity at the posttranslational level (15–20). Human genetics and clinical studies have emphatically demonstrated that mutations in the *ANGPTL4* gene (E40K) are associated with reduced plasma TAG and glucose levels (21–24). Importantly, the circulating level of ANGPTL4 is positively correlated with increased risk of cardiovascular disease (CVD) and T2D, along with obesity-associated diabetic phenotypes, such as high BMI, fat mass, and altered glucose homeostasis (25). These observations indicate that ANGPTL4 is strongly implicated in the development of metabolic diseases in humans.

Early work on ANGPTL4 in rodents was performed using whole-body transgenic or KO mouse models, thus limiting the ability to understand the specific role of ANGPTL4 in vital metabolic tissues. Therefore, some of the conclusions drawn from these studies have been contradictory (13, 21, 26–30). A number of groups have shown that loss of *Angptl4* using KO mouse models or monoclonal antibodies against ANGPTL4 results in mesenteric lymphadenopathy (inflammation of lymph nodes), chylous ascites, acute phase response, and severe gut inflammation upon high-fat diet (HFD) or Western-type diet (WD) feeding, leading to metabolic complications and reduced survival (26, 31). In these studies, it is not clear whether

Authorship note: AKS and BC contributed equally to this work.
Conflict of interest: The authors have declared that no conflict of interest exists.

Submitted: June 3, 2020; **Accepted:** July 8, 2021; **Published:** September 1, 2021.
Reference information: *J Clin Invest*. 2021;131(17):e140989.
https://doi.org/10.1172/JCI140989.

these effects of *Angptl4* deficiency are LPL dependent or independent. This warrants a need for mouse models that are not affected by these confounding factors. Our recent work has demonstrated an essential role for adipose-derived ANGPTL4 in regulating lipid uptake and regulation of metabolic function by AT (32). We and others have observed that AT-specific *Angptl4* KO (Ad-KO) mice displayed reduced circulating TAG levels, similar to what was observed in humans with a missense mutation in *ANGPTL4* (E40K variant) (32, 33). However, other factors identified in this study, such as body weight and regulation of glucose homeostasis, were unaltered after chronic administration of HFD feeding (32). These findings suggest that ANGPTL4 in other tissues, such as the liver, could also play a key role in the regulation of whole-body metabolism. Moreover, the physiological roles of ANGPTL4 in liver metabolism are primarily unclear. Therefore, we generated a hepatocyte-specific mouse model (hepatocyte-specific *Angptl4* mutant mice [*Hmut*]) in which exons 4–6 of *Angptl4* have been knocked out. Notably, we found that hepatocyte-specific depletion of *Angptl4* prevents diet-induced obesity, reduces circulating TAGs, attenuates ectopic lipid accumulation, enhances insulin sensitivity and glucose tolerance, and protects against the progression of atherosclerosis. Mechanistically, *Angptl4* deficiency in hepatocytes activates the hepatic lipase (HL), leading to an increased uptake of FA that results in ROS production and activation of AMPK in hepatocytes. Most importantly, therapeutic *Angptl4* expression inhibition of using *N*-acetylgalactosamine–conjugated (GalNac-conjugated) antisense oligonucleotides (*Angptl4*-ASO) improves metabolic homeostasis and prevents diet-induced obesity without eliciting any deleterious side effects.

Results

Hepatocyte-specific depletion of Angptl4 alters systemic lipid metabolism. While the metabolic function of AT-derived ANGPTL4 in regulating whole-body lipid and glucose metabolism have been recently elucidated, ANGPTL4 is also highly expressed in the human liver (Figure 1A), where its function is poorly understood. To understand the hepatocyte-specific role of ANGPTL4 on whole-body lipid and glucose metabolism, we generated conditional KO mice, which were then bred with Albumin-Cre animals to specifically deplete the expression of *Angptl4* in hepatocytes (*Hmut*). The LoxP sites only flank exons 4–6; therefore, we analyzed the mRNA levels of the individual exons (exons 1–7) of hepatic *Angptl4* through quantitative reverse-transcription PCR (qRT-PCR).

The expression of exons 1 to 3 and 7 was reduced by approximately 50%, whereas more than 95% reduction was observed for exons 4–6 in the liver of *Hmut* mice as compared with WT mice (Figure 1, B and C, and Supplemental Figure 1A; supplemental material available online with this article; https://doi.org/10.1172/JCI140989DS1), with no compensatory increase in the expression of either ANGPTL3 or ANGPTL8 (Supplemental Figure 1B). The expression of *Angptl4* was unaltered in white AT (WAT) and brown AT (BAT), reflecting the specific reduction of *Angptl4* in hepatocytes, with residual *Angptl4* mRNA present in Kupffer cells (KCs)/macrophages (Supplemental Figure 1C). The purification of the different cellular populations was confirmed by measuring the expression of specific genes by qRT-PCR (Supplemental Figure 1D). To assess whether hepatic *Angptl4* deficiency influences lipoprotein and glucose metabolism, we measured body weight and plasma levels of lipids and glucose in 2-month-old *Hmut* mice fed a chow diet (CD). Notably, we found a significant reduction in circulating TAGs, total cholesterol (TC), and HDL cholesterol (HDL-C) in *Hmut* mice (Figure 1D). We further confirmed these results by measuring TC and TAG in different lipoprotein fractions isolated by fast protein liquid chromatography (FPLC) (Figure 1E). Fasting blood glucose levels, body weight, and circulating nonesterified fatty acid (NEFA) levels were similar in both groups of mice (Supplemental Figure 1, E–G).

Absence of ANGPTL4 function in hepatocytes enhances hepatic lipid uptake. In order to understand how hepatocyte-derived ANGPTL4 regulates systemic lipid metabolism, we assessed possible causes of hypotriglyceridemia in *Hmut* mice. We reasoned that these effects could be due to either enhanced TAG-rich lipoprotein (TRL) (chylomicrons and VLDL) catabolism, reduction in hepatic VLDL production, or defective lipid absorption in the gut. To determine the impact of hepatocyte-specific suppression of *Angptl4* on the clearance of dietary TAGs (chylomicrons) in circulation, we administered mice with an intragastric gavage of olive oil, and plasma TAGs and FFAs were measured at indicated time points after gavage. We found that postprandial plasma levels of TAGs and FFAs were reduced in *Hmut* mice as compared with WT mice (Figure 2, A and B). To identify the tissue or tissues responsible for the enhanced lipid clearance, we analyzed lipid uptake using a [^{3}H]-oleate–labeled triolein tracer. Interestingly, *Hmut* mice displayed increased lipid uptake in the liver and accelerated clearance of circulating plasma lipid as compared with the WT control mice (Figure 2C). Next, we determined whether the accelerated clearance of TRL particles was a consequence of increased lipolytic activity. As such, we analyzed the HL and LPL activity in the plasma after heparin injection. Remarkably, *Hmut* mice had noticeably increased postheparin plasma HL activity compared with WT mice (Figure 2D). To determine which liver cell type was influencing postheparin plasma HL activity, we measured HL activity in primary hepatocytes and KCs. Primary hepatocytes, but not KCs, from *Hmut* mice had increased HL activity compared with hepatocytes and KCs isolated from WT mice (Supplemental Figure 2A). Although the HL activity was higher in hepatocytes derived from *Hmut* mice, the expression levels of HL in both hepatocytes and KCs were similar in *Hmut* and WT cells (Supplemental Figure 2B). Consistent with this finding, HL activity was markedly increased in the liver of *Hmut* as compared with WT mice (Supplemental Figure 2C). We then determined whether HL mediates TAG catabolism in *Hmut* mice. To achieve this, we treated *Hmut* mice with siRNA targeted against HL (siHL *Hmut*) or a control antisense nucleotide (siC *Hmut*). Consistent with the above findings, suppression of HL (Supplemental Figure 2D) normalized TAG levels in mice deficient in ANGPTL4 in hepatocytes (Supplemental Figure 2E). In addition to differences in HL activity, we found a modest increase in postheparin plasma LPL activity in *Hmut* compared with WT mice (Figure 2E). LPL activity was also significantly increased in the liver, but not in other tissues with high LPL expression, such as ATs (WAT and BAT), heart, and muscle (Supplemental Figure 2F). Similarly to what occurred with HL, LPL activity was significantly increased in hepatocytes, but not in KCs, of *Hmut* compared with WT mouse primary cells (Supplemental Figure 2G), while expression of the enzyme was not affected (Supplemental Figure 2H). Finally, we analyzed whether hepatic VLDL secretion and fat absorption also contributed to the reduction in

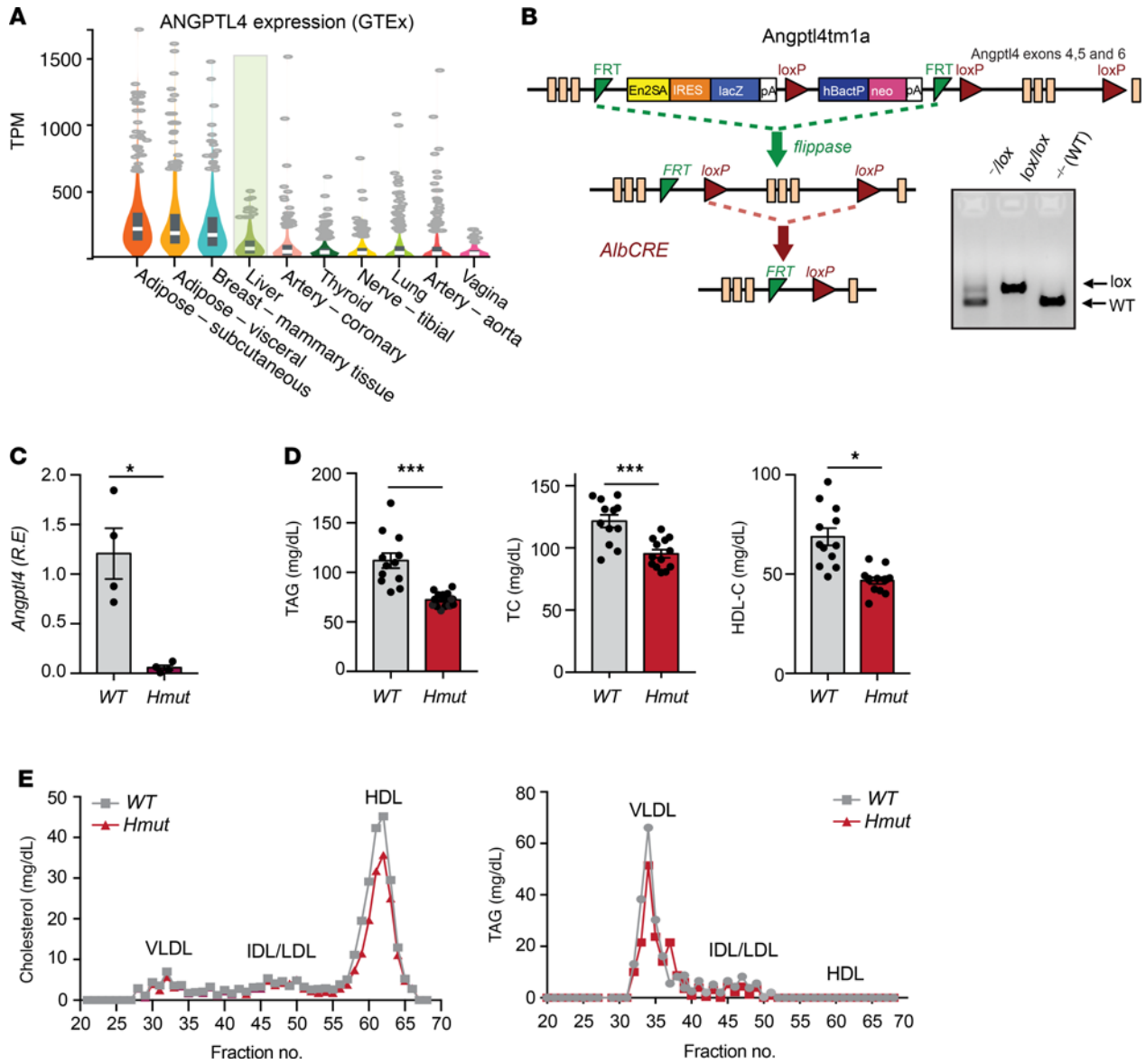

Figure 1. The loss of ANGPTL4 function in hepatocytes improves serum lipid profile. (**A**) Analysis of human ANGPTL4 expression in different tissues using Genotype-Tissue Expression (GTEx) database. Liver is highlighted. TPM, transcript per million reads. (**B**) Schematic diagram illustrating the generation of hepatocyte-specific ANGPTL4 mutant (*Hmut*) mice. The construct is composed of a short flippase recombination enzyme (Flp) recognition target (FRT), reporter, and a Cre recombinase recognition target (loxP). Angptl4 exons 4–6 are flanked by the lox P site. Mice with the floxed allele were generated by crossing with flp recombinase-deleter mice (middle panel). Subsequently, these mice were bred with mice expressing Cre recombinase to produce tissue-specific *Hmut* mice (bottom panel). PCR amplification of *Angptl4*$^{fl/fl}$ mice displaying bands from both, 1, or none of the floxed alleles (right panel). (**C**) mRNA expression of *Angptl4* in the liver of WT and *Hmut* mice. R.E., relative expression. (**D**) Fasted plasma TAG (left panel), TC (middle panel), and HDL-C (right panel) from overnight-fasted WT and *Hmut* mice fed CD for 2 months (n = 10–13). (**E**) Cholesterol (left panel) and TAG (right panel) content of FPLC-fractionated lipoproteins from pooled plasma of overnight-fasted WT and *Hmut* mice fed a CD for 2 months (n = 7). All data are represented as mean ± SEM. *P < 0.05; ***P < 0.001, comparing *Hmut* with WT mice using the unpaired t test.

circulating TAGs observed in *Hmut* mice. As shown in Figure 2, F and G, VLDL production and fat absorption were not affected by ANGPTL4 expression in hepatocytes. Together, these data indicate that hepatocyte-specific loss of ANGPTL4 results in reduced circulating TAGs, likely due to enhanced hepatocyte HL- and LPL-mediated lipolysis and clearance of TRL.

Lack of ANGPTL4 in the hepatocytes reduces body weight, fat mass, and hepatic neutral lipid accumulation. Elevated circulating TAGs might cause ectopic lipid deposition, leading to IR (5, 7, 10, 34, 35). Therefore, we tested to determine whether hepatocyte-specific depletion of ANGPTL4 could protect against diet-induced obesity and glucose intolerance after feeding mice an HFD for 16 weeks. We observed that *Hmut* mice gained significantly less weight than WT mice (Figure 3A). The difference in body weight was independent of food intake, which was similar in both groups of mice (Supplemental Figure 3A). This was accompanied by lower total body fat mass, fat weight, and adipocyte cell size in the *Hmut* mice (Figure 3, B–D). Similarly to mice fed a CD, *Hmut* mice fed an

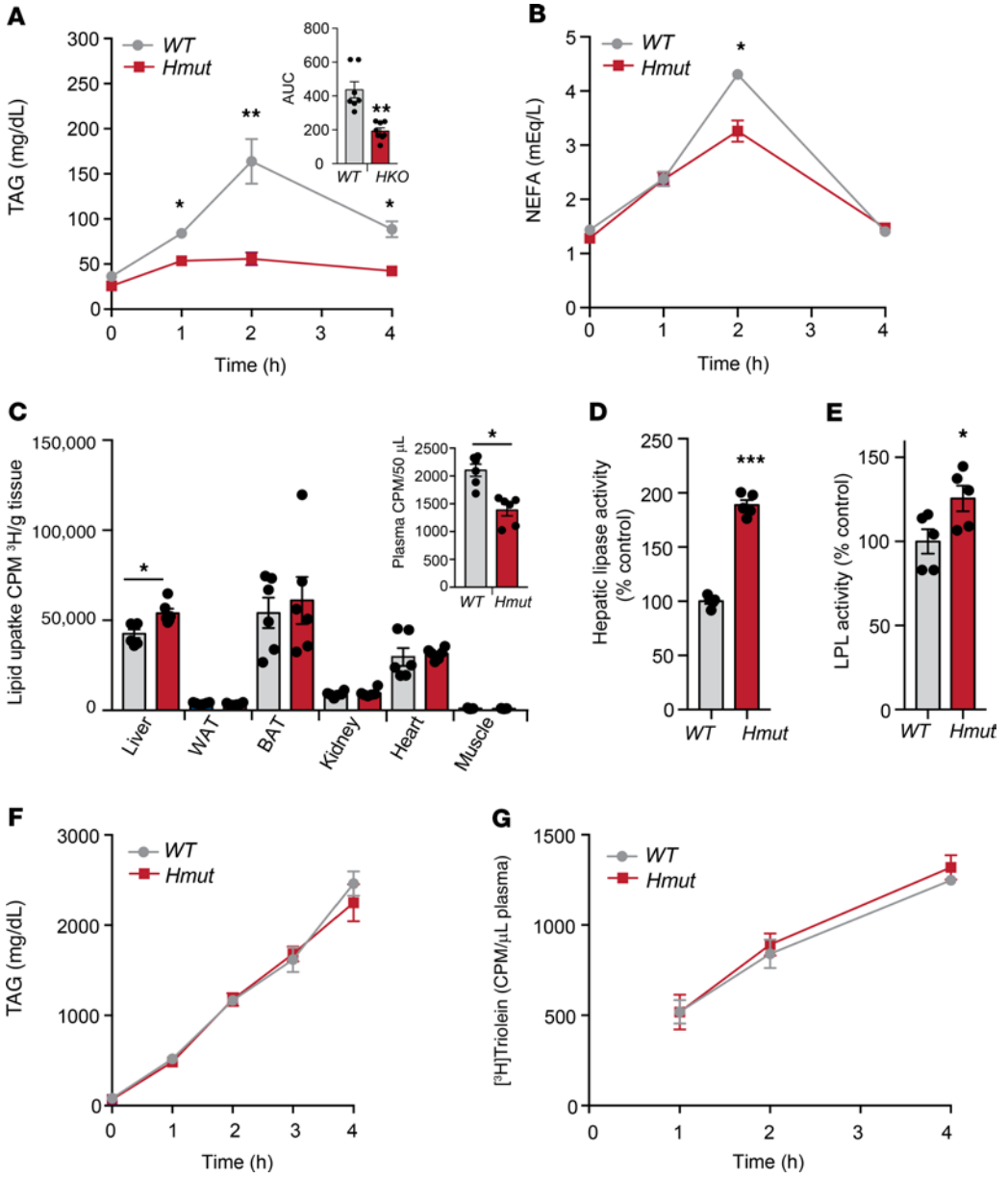

Figure 2. Inactivation of ANGPTL4 in hepatocytes enhances plasma TAG clearance and hepatic lipid uptake. (**A** and **B**) Oral lipid tolerance test showing the clearance of TAG and NEFA from the plasma of WT and *Hmut* mice fasted for 4 hours, followed by oral gavage of olive oil. Inset represents the AUC. (**C**) Radioactivity incorporation in indicated tissues after 2 hours of oral gavage of [^{3}H]-labeled triolein in WT or *Hmut* mice fasted for 4 hours. Inset represents plasma lipid clearance. (**D** and **E**) HL and LPL activity in the postheparin plasma from overnight-fasted WT and *Hmut* mice. (**F**) Plasma TAG from overnight-fasted WT and *Hmut* mice treated with plasma LPL inhibitor poloxamer 407 to inhibit the hydrolysis of circulating TAG (n = 5). (**G**) Serum ^{3}H-labled triolein counts after injection of poloxamer 407 combined with oral lipid gavage containing ^{3}H-labeled triolein (n = 5). All data are represented as mean ± SEM. *P < 0.05; **P < 0.01; ***P < 0.001, comparing *Hmut* with WT mice using the unpaired t test.

HFD showed reduced plasma TAGs, TC, and HDL-C levels when compared with WT control mice (Figure 3E). These results were further confirmed by FPLC analysis (Figure 3F). Since alterations in body fat mass are often associated with changes in lipid accumulation in the liver (3, 36, 37), we determined neutral lipid content in the liver of *Hmut* and WT mice. As anticipated, we noticed a significant decrease in the liver weight of *Hmut* mice as compared with WT mice (Figure 3G). Oil red O and H&E staining of liver sections indicated reduced accumulation of neutral lipids in the liver of *Hmut* mice (Figure 3H), which was further confirmed by measuring TAG content in the liver (Figure 3I).

Elevated lipid deposition in the liver promotes the induction of hepatic inflammation (11). Therefore, we investigated whether loss of *Angptl4* in hepatocytes influences hepatic inflammation under HFD-fed conditions. We first analyzed the distribution of monocytes and KCs in the liver of mice challenged with HFD for 16 weeks. FACS analysis showed that lack of hepatocyte *Angptl4* reduced the proportion of monocytes in the liver, whereas we did not observe any differences in KCs between genotypes (Supplemental Figure 3B). We also found a significant reduction in acute-phase response (APR) genes, including serum amyloid A (*Saa*), haptoglobin (*Hp*), and lipocalin 2 (*Lcn2*), that arise from

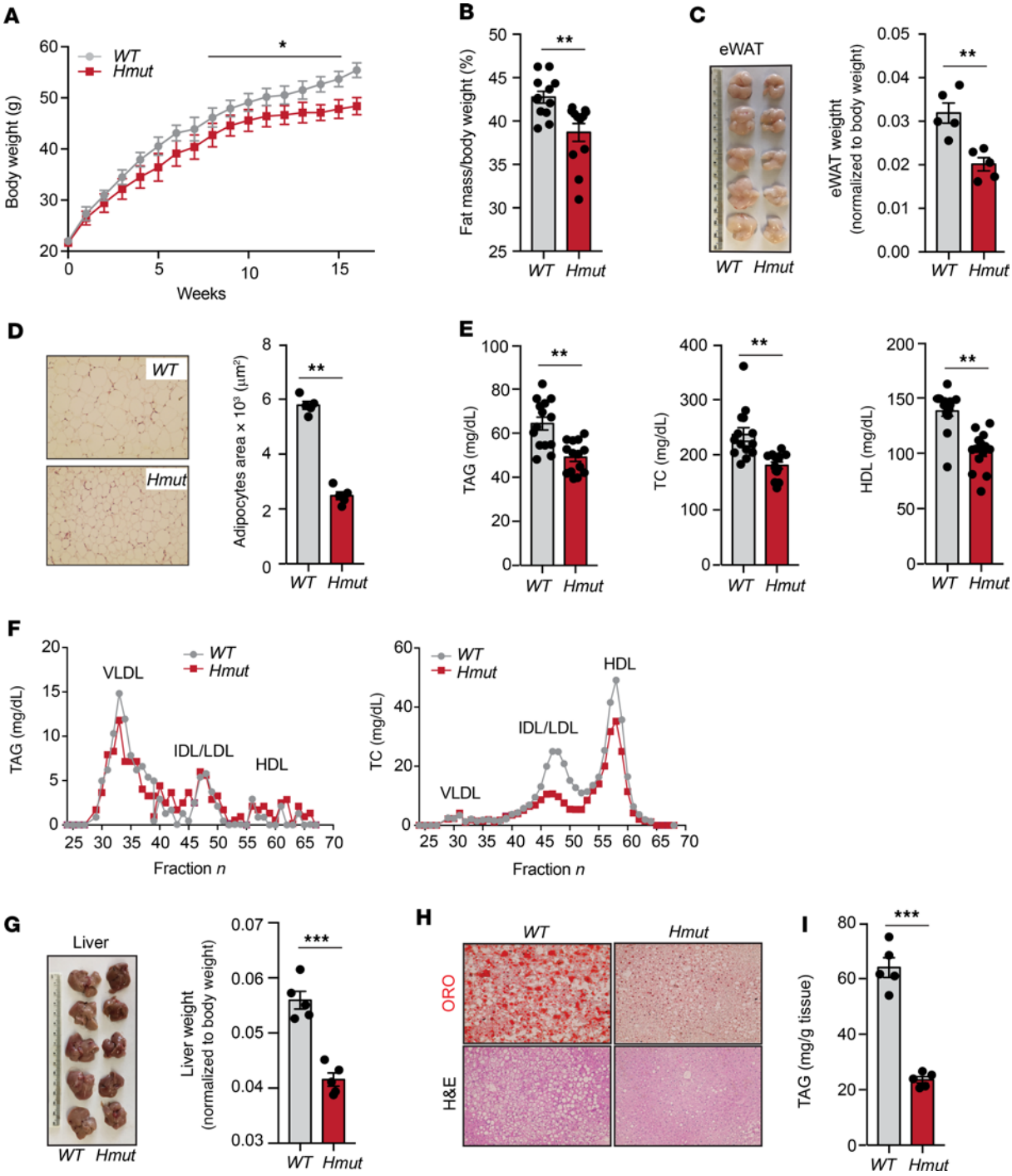

Figure 3. Hepatic ANGPTL4 deficiency protects from diet-induced obesity and decreases hepatic lipid accumulation. (**A** and **B**) Body weight and fat mass measured by Echo-MRI of WT and *Hmut* mice fed an HFD for 16 weeks (n = 10–13). (**C** and **D**) Fat epididymal WAT (eWAT) weight, representative images of H&E sections of WAT, and quantification of adipocyte size isolated from WT and *Hmut* mice fed an HFD for 16 weeks. Original magnification, ×10. (**E**) Levels of TAG, TC, and HDL-C in the plasma of overnight -fasted WT and *Hmut* mice fed an HFD for 16 weeks. (**F**) FPLC analysis of lipoprotein profile from pooled plasma of overnight-fasted WT and *Hmut* mice (n = 5). (**G**–**I**) Representative images of the liver and liver weight (**G**), representative photographs of oil red O–stained (ORO) and H&E-stained sections of liver isolated from WT and *Hmut* mice fed HFD for 16 weeks (**H**), and hepatic TAG levels (**I**). Original magnification ×20. All data are represented as mean ± SEM. $^*P < 0.05$; $^{**}P < 0.01$; $^{***}P < 0.001$, comparing *Hmut* with WT mice using the unpaired t test.

inflammation (38) in livers from *Hmut* compared with WT mice (Supplemental Figure 3C). Moreover, circulating serum amyloid A (SAA) levels were similar between both groups of mice (Supplemental Figure 3D). Consistent with these findings, *Hmut* mice did not show inflamed mesenteric lymph node (MLN) or Touton giant cells under HFD-feeding conditions (Supplemental Figure 3E). Taken together, these data indicate that hepatic ANGPTL4 controls lipoprotein metabolism and its absence improves the metabolic health of mice under pathophysiological conditions, such as diet-induced obesity.

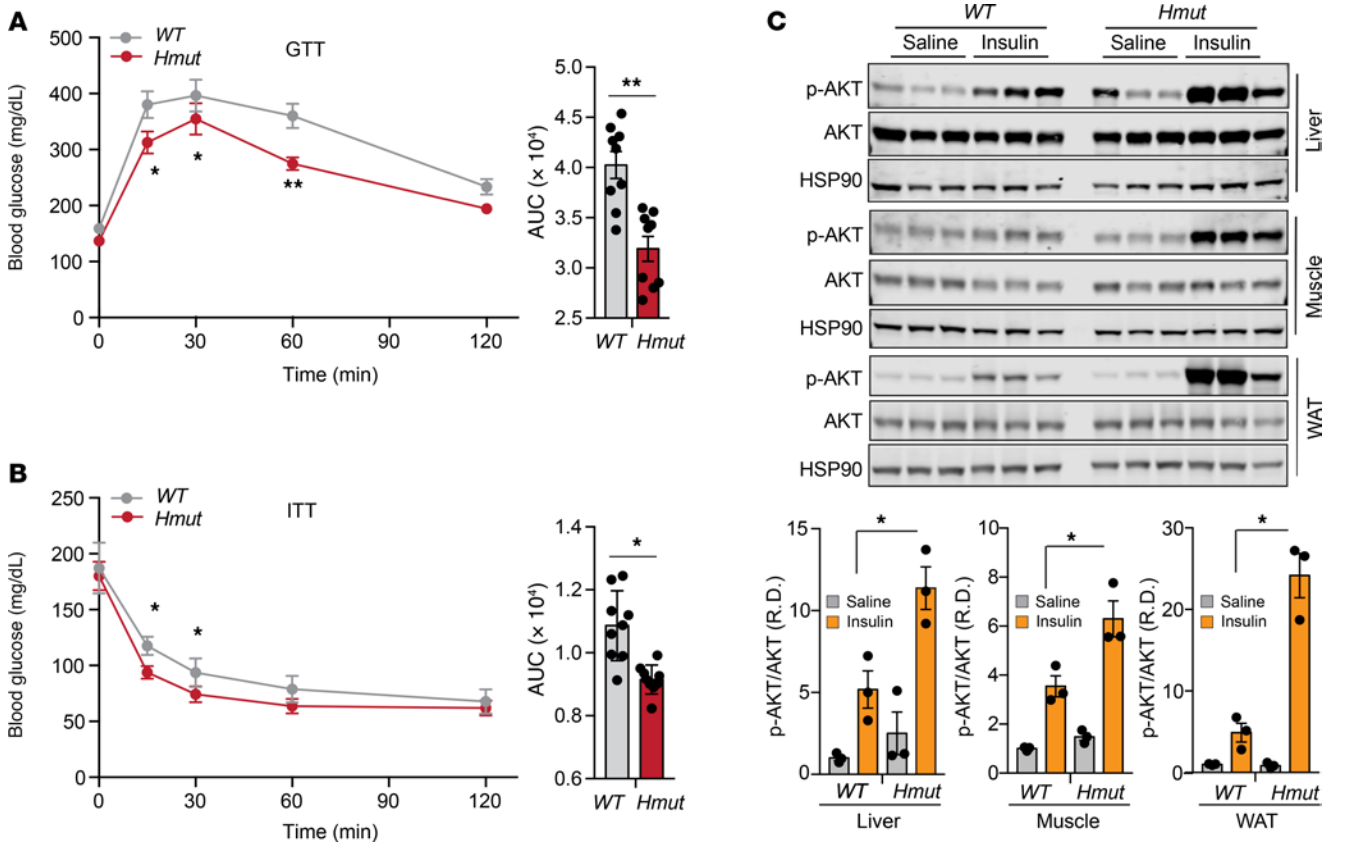

Figure 4. Lack of ANGPTL4 function in hepatocytes results in improved glucose homeostasis and enhanced insulin sensitivity. (**A**) Intraperitoneal glucose tolerance test (GTT) (1 g/kg body weight) and AUC (right panels) of mice fed an HFD for 16 weeks. (**B**) Intraperitoneal insulin tolerance test (ITT) (2.0 U/kg body weight) and AUC (right panels) of mice fed an HFD for 16 weeks. (**C**) Representative immunoblot images and quantification of Akt (Ser 473 phosphorylation status relative to total AKT) (right panels) in the liver, muscle, and AT 15 minutes after an intraperitoneal bolus of insulin (2.0 U/kg) or saline in 16-week HFD-fed WT versus *Hmut* mice. R.D., relative density. All data are represented as mean ± SEM. $^*P < 0.05$; $^{**}P < 0.01$, comparing *Hmut* with WT mice using unpaired *t* test.

Loss of function of ANGPTL4 in hepatocytes improves glucose homeostasis and enhances insulin sensitivity in metabolic tissues. Recent studies on humans and mice have reported that loss of function of *ANGPTL4* is associated with improved glucose tolerance and insulin sensitivity (21, 27). Since diet-induced obesity is often accompanied by IR-linked glucose intolerance, we assessed the net functional outcome of hepatic *Angptl4* deficiency on systemic glucose metabolism during diet-induced obesity. We found that *Hmut* mice showed remarkably improved glucose tolerance and insulin sensitivity compared with WT mice after 16 weeks of HFD feeding (Figure 4, A and B). To further evaluate insulin sensitivity in different metabolic tissue(s), we assessed the levels of phosphorylated AKT (p-AKT) following insulin treatment. The results showed a markedly increased p-AKT/AKT ratio in skeletal muscle, AT, and liver of *Hmut* mice following intraperitoneal injection of insulin (Figure 4C), again suggesting enhanced insulin sensitivity in hepatocyte *Angptl4*-deficient mice.

Reduced body weight and circulating lipids are associated with attenuated atherosclerosis in hypercholesterolemic mice. Human genetic studies have shown an association between loss-of-function variants of *ANGPTL4* and reduced risk of CVD (24). Our results show that loss of *Angptl4* in hepatocytes markedly reduces circulating apoB-containing lipoproteins and improves glucose homeostasis, suggesting that suppression of *Angptl4* in hepatocytes might protect against the progression of atherosclerosis. To test this hypothesis, we injected *Hmut* and WT mice with an AAV8-PCSK9 adenoviral vector encoding a gain-of-function mutation in PCSK9 that degrades the LDL receptor (LDLR) and induces hyperlipidemia. These mice were then fed a WD for 16 weeks to induce atherosclerotic plaque formation (32). Consistent with the phenotype observed in HFD-fed mice, we found that *Hmut* mice were resistant to weight gain with no change in food intake upon WD feeding, which was reflected in reduced fat mass as compared with WT (Figure 5A and Supplemental Figure 4, A and B). While circulating HDL-C levels were unaltered, we observed a significant reduction in plasma TAGs and TC levels as well as fasting blood glucose in *Hmut* mice 16 weeks after WD feeding (Figure 5B and Supplemental Figure 4, C and D). FPLC analysis revealed decreased TAG and cholesterol levels in VLDL fractions and cholesterol in intermediate-density lipoprotein (IDL)/LDL fractions of *Hmut* compared with WT mice (Figure 5C). Similarly to what we observed in mice lacking *Angptl4* in AT (32), deficiency of *Angptl4* in hepatocytes also led to a significant reduction in atherogenesis when compared with WT littermates, as indicated by the reduced aortic root plaque area and diminished accumulation of neutral lipids, as assessed by oil red O staining (Figure 5D). Furthermore, we also observed significantly decreased neutral lipid accumulation in the whole aorta of *Hmut* compared with WT mice (Supplemental Figure 4E). The reduced lipid deposition in the aorta of *Hmut* mice

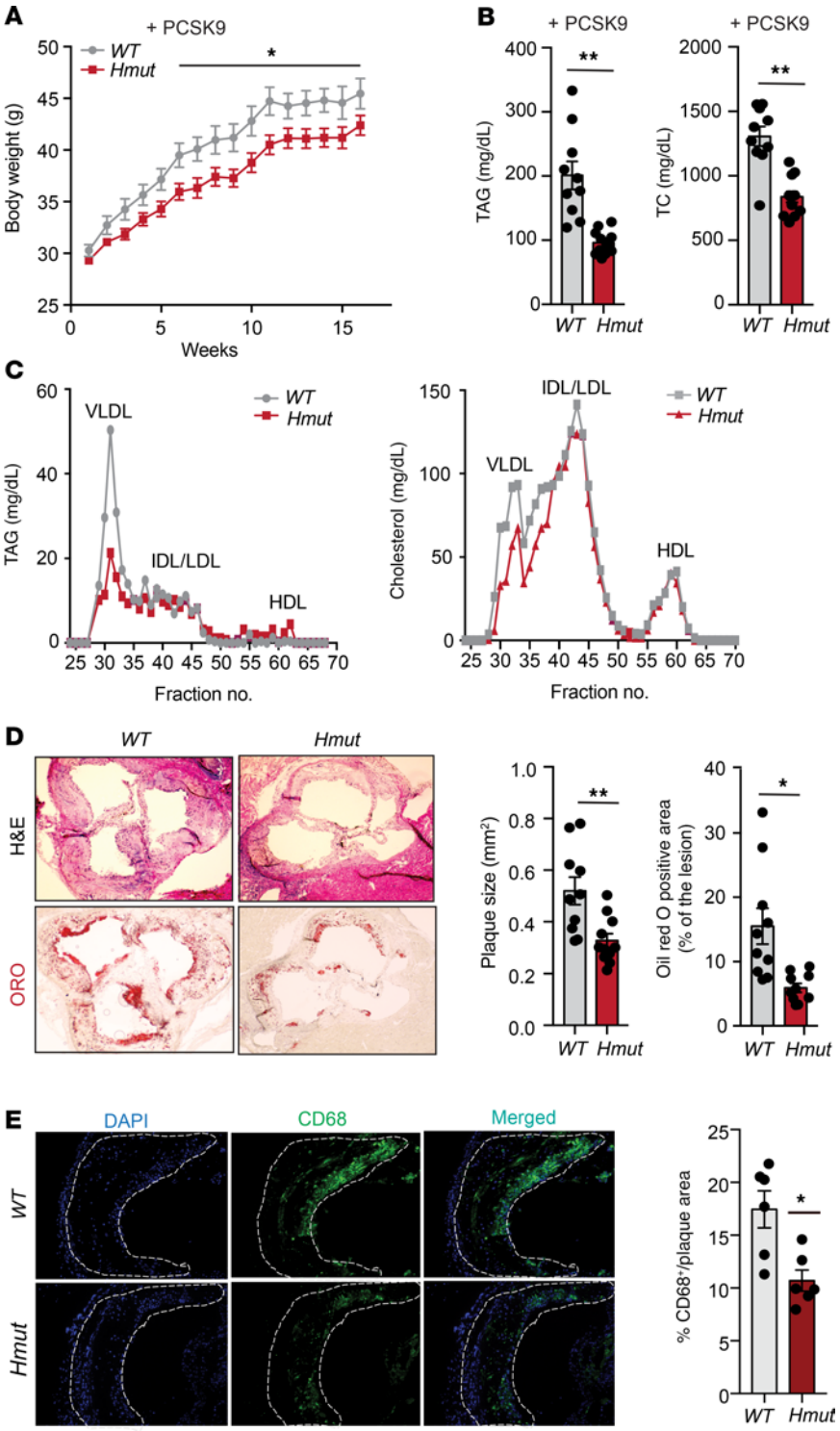

Figure 5. Genetic loss of ANGPTL4 in hepatocytes improves obesity and attenuates atherosclerosis. (**A**) Body weight (**B**), plasma TAGs, and TC from overnight-fasted WT and *Hmut* mice fed a WD for 16 weeks. (**C**) Lipoprotein profile analysis of pooled plasma of overnight-fasted WT and *Hmut* mice (n = 5). (**D**) Left: representative histological analysis of a cross section of the aortic root sinus isolated from WT and *Hmut* mice fed a WD for 16 weeks stained with H&E (upper panels) and oil red O (lower panels). Right: quantification of plaque size and the percentage area of neutral lipid accumulation calculated from H&E or ORO cross sections, respectively. Original magnification, ×10. (**E**) Representative cross-section analysis of macrophage content (CD68-positive cells) of the aortic root from WT and *Hmut* mice fed a WD for 16 weeks. Quantifications of the graphs on the right. Original magnification, ×10. All data are represented as mean ± SEM. $^*P < 0.05$; $^{**}P < 0.01$, comparing *Hmut* with WT mice using the unpaired t test.

was accompanied by a marked reduction in vascular inflammation, as shown by the significant decrease in macrophage accumulation in the lesions (Figure 5E). However, this effect was not accompanied by any significant difference in circulating blood leukocytes or proinflammatory monocytes (Ly6C^{hi}) (Supplemental Figure 4F) nor plasma SAA levels between the groups (Supplemental Figure 4G). Taken together, these results demonstrate that loss of function of ANGPTL4 in hepatocytes protects against diet-induced obesity and atherosclerosis.

Hepatocyte-specific loss of ANGPTL4 suppresses the endogenous lipogenic pathway and promotes oxidative metabolism via AMPK activation. We next investigated the potential mechanisms by which loss of *Angptl4* in hepatocytes reduced hepatic lipid accumulation despite increased lipid uptake. To this end, we first analyzed the expression and activity of the main enzymes involved in DNL, including acetyl CoA carboxylase (ACC), FA synthase (FASN), and HMG-CoA reductase (HMGCR) (39, 40). Notably, ACC phosphorylation as well as FASN and HMGCR expression and activity were significantly reduced in the liver of *Hmut* mice as compared with WT mice fed a CD or HFD (Figure 6, A–C, and Supplemental Figure 5, A and B). In addition to the reduction in the activity of key enzymes involved in DNL, we also observed a marked increase in FAO in liver tissue isolated from *Hmut* mice (Figure 6D). We next studied the activation state of AMPK, which has been previously reported to be regulated by FA (41) and ANGPTL4 (42), and coordinates FA partitioning between oxidation and biosynthesis pathways by increasing FAO capacity and inhibiting DNL (43). Notably, we found a significant increase in AMPK phosphorylation (activated form) in the liver of *Hmut* mice as compared with WT (Figure 6E). To assess whether enhanced lipid uptake mediated the AMPK activation in *ANGPTL4*-depleted human hepatoma cells, we generated stable clones of HepG2 cells by lentiviral-mediated transduction of specific shRNAs against *Angptl4*. ANGPTL4 mRNA and protein expression (measured in the cell culture media) were significantly reduced in *Angptl4* shRNA–transduced cells compared with control cells (Supplemental Figure 6, A and B). The specificity of ANGPTL4 measurements was confirmed in HepG2 treated with hypoxia mimetics ($CoCl_2$), which induced the expression of ANGPTL4, and in HUVECs, known to express *ANGPTL4* (Supplemental Figure 6B). Consistent with our in vivo findings, suppression of

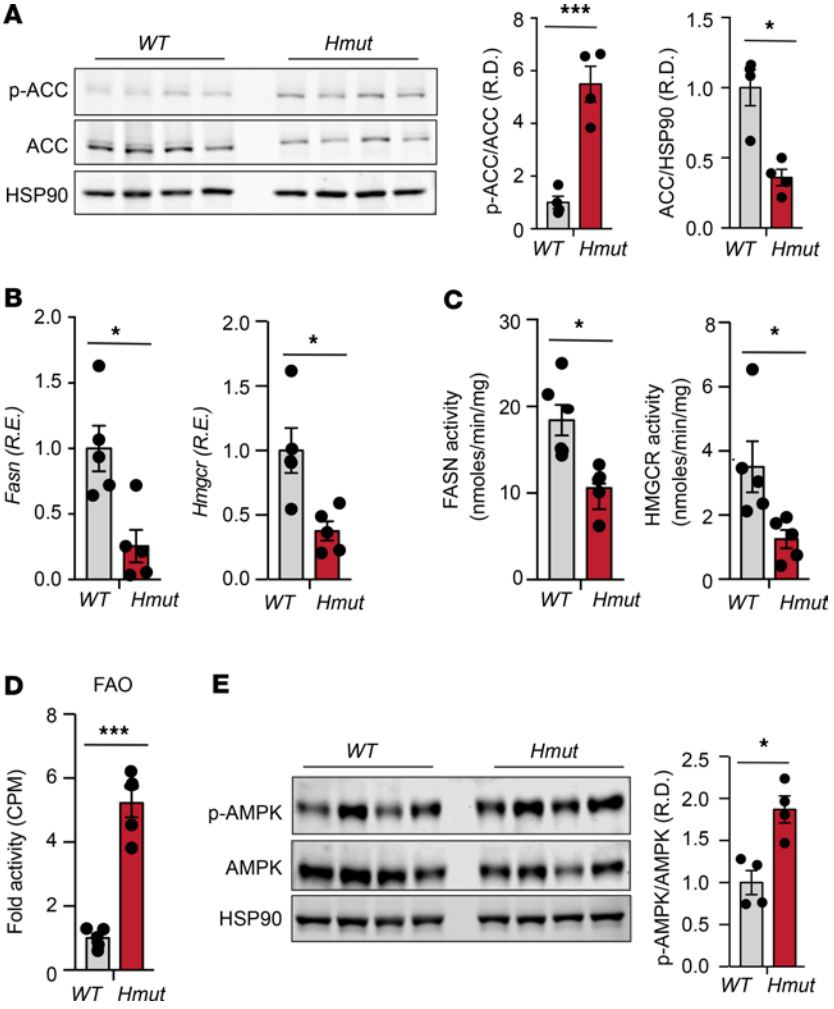

Figure 6. Loss of ANGPTL4 in hepatocytes inhibits DNL pathway and promotes FAO. (**A**) Representative immunoblot images showing p-ACC and ACC levels in the liver isolated from fasted WT and *Hmut* mice fed a CD for 8 weeks. The right panel shows p-ACC/ACC and ACC/HSP90 ratios from immunoblot image quantification. (**B**–**D**) Expression and respective activity of the enzymes FASN and HMGCR and FAO in liver isolated from fasted mice. (**E**) Immunoblot images of p-AMPK and total AMPK protein in liver isolated from fasted mice. Densitometric analysis shown in the right panels. All data are represented as mean ± SEM. $^*P < 0.05$; $^{***}P < 0.001$, comparing *Hmut* with WT mice using unpaired *t* test.

ANGPTL4 expression resulted in enhanced FA uptake in HepG2 cells (Figure 7A). To determine the contribution of HL to the lipid uptake and FA-mediated AMPK activation observed in *ANGPTL4*-silenced HepG2 cells, we silenced *HL* (Supplemental Figure 6B, right panel) and analyzed lipid uptake and AMPK activation. We found that increased lipid uptake and AMPK phosphorylation, in response to reduced expression of *ANGPTL4* (shANGPTL4), were diminished upon silencing of *HL* (Figure 7, B and C). These results suggest that increased HL activity mediates AMPK activation, likely due to enhanced lipid uptake.

Previous work has implicated ROS in the activation of AMPK (44, 45), and increased FAO promotes ROS generation (46). Therefore, we next assessed whether *ANGPTL4* silencing increases ROS production and AMPK activation in HepG2 cells. As shown in Figure 7D, ANGPTL4 suppression in HepG2 cells results in a significant increase in dihydroethidium (DHE) staining, indicating higher ROS levels. This effect on ROS levels was attenuated when cells were treated with etoximir (Figure 7D), an FAO inhibitor (47), suggesting that elevated ROS was a consequence of increased FAO. To determine whether the increased FAO observed in ANGPTL4 depleted cells was mediated by HL-regulated TAG lipolysis and FA uptake, we silenced *HL* in shC and shAngptl4 transduced cells. The results showed that genetic silencing of *HL* attenuates ROS production in cells lacking ANGPTL4 (Figure 7E), suggesting that enhanced FA uptake in the absence of ANGPTL4 contributes to the generation of ROS. Next, we asked whether the increase in ROS levels may serve to further promote sustained AMPK activation. To this end, we treated control and *ANGPTL4*-deficient cells with *N*-acetyl-L-cysteine (NAC), which is commonly used to scavenge ROS, and compound C (CompC), an inhibitor of AMPK. NAC treatment attenuated the increased ROS accumulation, AMPK phosphorylation, and FAO observed in ANGPTL4-depleted cells (Figure 7, F–H). Most importantly, direct inhibition of AMPK blunted the increased FAO in HepG2 cells transduced with shAngptl4 (Figure 7, F and H), which correlated with a significant reduction in FAO-associated genes (Supplemental Figure 6C). In contrast, the expression of *ACC*, *FASN*, and *HMGCR* was downregulated in *ANGPTL4*-deficient hepatoma cells, which was normalized with either CompC or NAC (Supplemental Figure 6D). Suppression of the lipid biosynthetic genes was associated with diminished mTORC1-mediated SREBP1 activation (Supplemental Figure 6E). These findings suggest that negative regulation of mTORC by AMPK (48, 49) controls the expression of genes associated with lipid biosynthesis. Indeed, inhibition of AMPK or suppression of ROS using CompC and NAC, respectively, attenuated this effect.

We next assessed whether ROS-mediated AMPK activation is involved in mediating the effects of *Angptl4* deficiency on hepatic FA metabolism in vivo. To this end, we administered *Hmut* mice with either CompC or NAC. Treatment with NAC reduced ROS levels in primary hepatocytes isolated from *Hmut* mice (Figure 8, A and B). Most importantly, CompC or NAC suppressed the increase in AMPK and ACC phosphorylation, FAO, and the expression of genes involved in FAO (e.g., *Pgc-1α*, *Cpt1a*, *Crot*, and *Hadhb*) observed in *Hmut* mice (Figure 8, C–E). In contrast, the downregulation of DNL enzyme activity and the mRNA levels of *Acc*, *Fasn*, and *Hmgcr* found in primary hepatocytes from *Hmut* mice were significantly attenuated after CompC or NAC treatment (Figure 8, F–H). Taken together, these results suggest that increased lipase-mediated FA uptake in response to the absence of ANGPTL4 function in hepatocytes causes a compensatory increase in AMPK activation and FAO, which leads to increased ROS production, further promoting sustained activation of AMPK (Figure 8I).

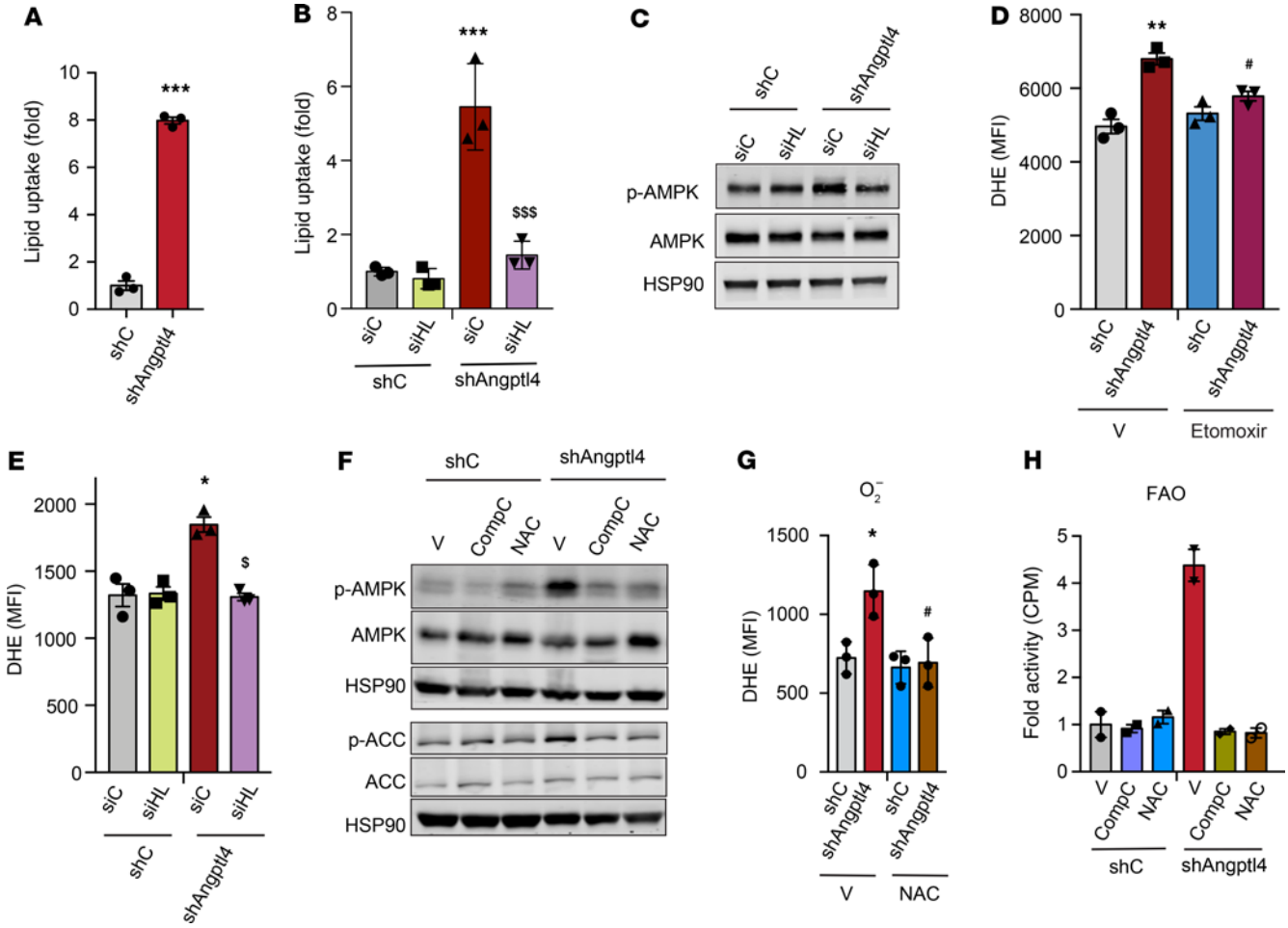

Figure 7. Inhibition of ROS and AMPK in HepG2 cells abrogates effect of ANGPTL4 in lipid metabolism. (**A** and **B**) HepG2 cells were stably transfected with 3 different shRNAs against *ANGPTL4* and HL expression transiently suppressed transfecting cells with specific siRNAs. HepG2–shC or HepG2-shAngptl4 cells transfected with HL or nonsilencing (NS) siRNAs were treated with radiolabeled chylomicron for 2 hours. Graph shows lipid uptake as a fold change of control (shC). (**C**) Representative immunoblot images showing the levels of p-AMPK, AMPK, and HSP90 in HepG2-shC and HepG2-sh shAngptl4 cells transfected with HL or nonsilencing (NS) siRNAs grown under conditions similar to those mentioned in **B**. (**D**) Relative ROS levels in HepG2-shC and HepG2-shNAGPTL4 cells treated with either DMSO or Etomoxir (40 μM) for 12 hours. (**E**) Relative ROS generation in cells used in **B** and **C**. (**F**) Representative immunoblot images showing the levels of p-AMPK, AMPK, p-ACC, ACC, and HSP90 in HepG2-shC and HepG2-shNAGPTL4 cells treated with or without CompC (20 μM) or NAC (5 mM) for 24 hours. (**G**) Relative ROS levels in HepG2-shC and HepG2-shNAGPTL4 cells treated with or without NAC (5 mM) for 24 hours. (**H**) FAO in cells under condition described in **F**. All data are represented as mean ± SEM. $^{*}P < 0.05$, HepG2-shANGPTL4 vs. HepG2-shC; $^{**}P < 0.01$, HepG2-shANGPTL4 vs. HepG2-shC; $^{***}P < 0.001$, HepG2-shANGPTL4 vs. HepG2-shC; $^{\$}P < 0.05$, HepG2-shANGPTL4–vehicle Ctrl versus HepG2-shANGPTL4 -NAC; $^{\$\$}P < 0.01$, HepG2-shANGPTL4–vehicle Ctrl versus HepG2-shANGPTL4 -NAC; $^{\#}P < 0.05$, HepG2-shANGPTL4 –vehicle Ctrl versus HepG2-shANGPTL4-CompC. *P* values were determined by 2-way ANOVA followed by Bonferroni's post hoc analysis.

Finally, we studied whether excess lipid uptake in the hepatocytes owing to the elevated HL activity in the absence of ANGPTL4 might promote ER stress response, which could lead to increase ROS production (50) and IR (51, 52). Interestingly, we observed decreased levels of some of the key ER stress markers, such as XBP1 and CHOP, in the liver of *Hmut* as compared with WT mice (Supplemental Figure 7, A and B). Furthermore, we did not observe significant effect on unfolded protein response–mediated (UPR-mediated) activation of ER oxidoreductin-1 (ERO1) and mitochondrial Ca^{2+} levels (Supplemental Figure 7, B and C), which affects mitochondrial membrane potential and elevates mitochondrial ROS production (50). These data suggest that the elevated ROS under *ANGPTL4* deficiency is independent of lipid loading–mediated ER stress/UPR.

GalNac-conjugated Angptl4 ASO reduces circulating TAGs, improves glucose tolerance, and protects against diet-induced obesity. Human genetic studies have shown that loss-of-function mutations in the *ANGPTL4* locus are associated with reduced T2D and risk of CVD (21, 22, 25). Given the beneficial metabolic effects observed in mice lacking *Angptl4* in hepatocytes, we evaluated whether a targeted inhibition of *Angptl4* expression in the liver improves metabolic homeostasis. To this end, we treated mice with GalNac-conjugated ASO against *Angptl4*. These constructs have a high affinity for the hepatocyte-specific asialoglycoprotein receptor; therefore, its conjugation allows specific inhibition of a target gene in the liver (53). Ten-week-old male C57BL/6 mice were administered with GalNac-conjugated *Angptl4* ASOs or GalNac-control ASOs (Ctrl ASO) via retroorbital injection once a week for 6 weeks under

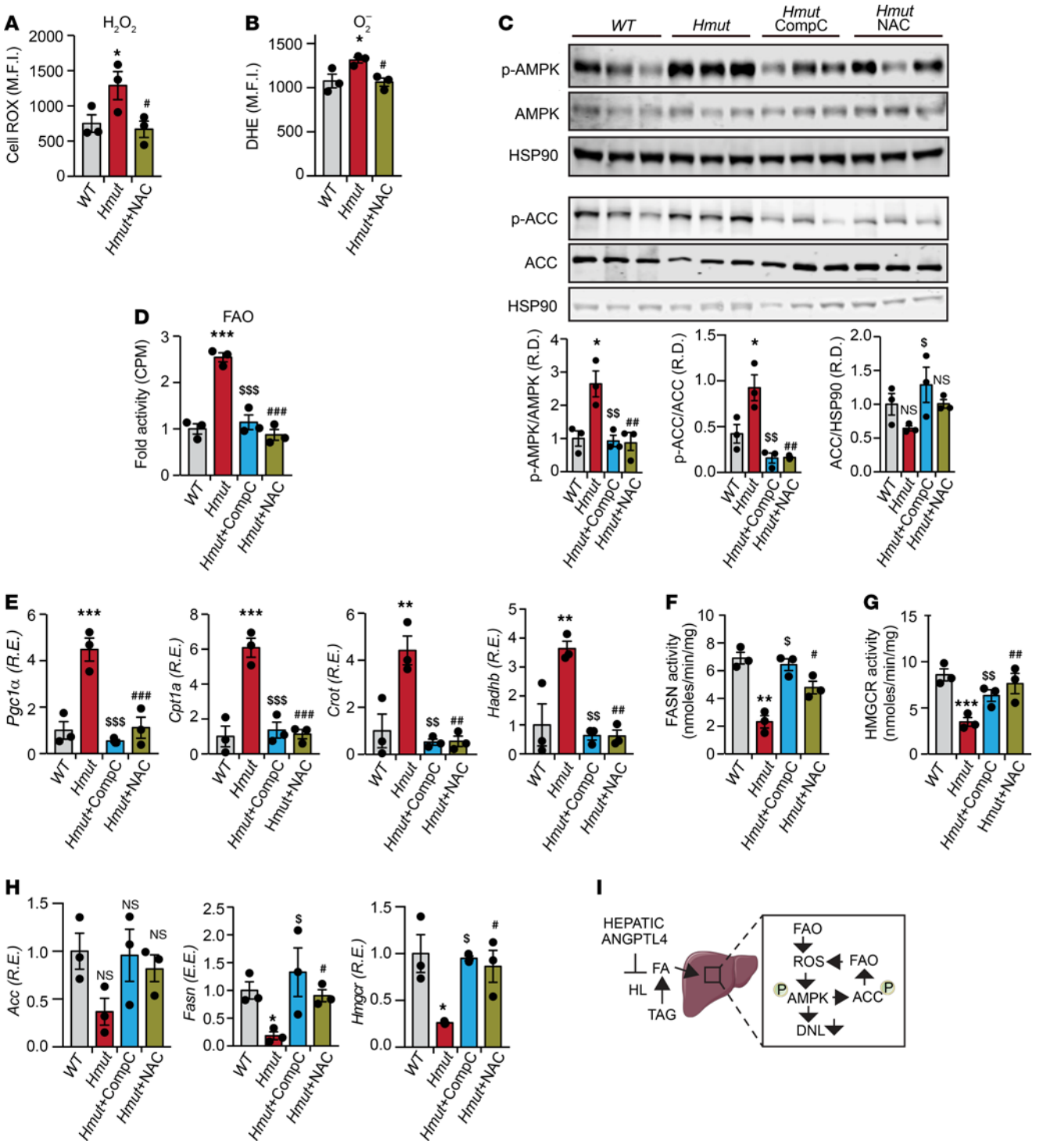

Figure 8. Inhibition of ROS-dependent activation of AMPK in *Hmut* mice reverses hepatic lipid metabolism. Eight-week-old *Hmut* mice were divided randomly into 3 groups. Each group of mice was administered with vehicle control (V), CompC, and NAC, respectively, for 3 consecutive days. (**A** and **B**) Determination of cellular ROS (H_2O_2 and O_2^-) in the hepatocytes isolated from the *Hmut* mice with indicated treatment groups. (**C**) Immunoblots showing the levels of p-AMPK, AMPK, p-ACC, and ACC in the liver isolated from fasted *Hmut* mice from indicated treatment groups. Lower panel shows image quantification of p-AMPK/AMPK, p-ACC/ACC, and ACC/HSP90 ratios from immunoblot densitometry. (**D**) FAO in liver of fasted *Hmut* mice from indicated treatment groups. (**E**) mRNA expression profile of FAO genes. (**F** and **G**) FASN and HMGCR enzymatic activity in the liver. (**H**) FA biosynthesis genes in the liver of mice administered with indicated inhibitors, as assessed by qRT-PCR. All data are represented as mean ± SEM. $^*P < 0.05$, WT versus *Hmut* mice; $^{**}P < 0.01$, WT versus *Hmut* mice; $^{***}P < 0.001$, WT versus *Hmut* mice; $^{\$}P < 0.05$, *Hmut*-Ctrl versus *Hmut*-NAC; $^{\$\$}P < 0.01$, *Hmut*-Ctrl versus *Hmut*-NAC; $^{\$\$\$}P < 0.001$, *Hmut*-Ctrl versus *Hmut*-NAC; $^{\#}P < 0.05$, *Hmut*-Ctrl versus *Hmut*-CompC; $^{\#\#}P < 0.01$, *Hmut*-Ctrl versus *Hmut*-CompC; $^{\#\#\#}P < 0.001$, *Hmut*-Ctrl versus *Hmut*-CompC. *P* values were determined by 1-way ANOVA followed by Bonferroni's post hoc analysis. (**I**) Proposed mechanism for the role of liver-derived ANGPTL4 in hepatic lipid metabolism.

CD-fed conditions (Figure 9A). Six weeks after treatment, *Angptl4* mRNA levels were markedly decreased in the liver without affecting *Angptl4* expression in KCs and AT (Figure 9B and Supplemental Figure 8A). Similar to the results observed in the hepatocyte-specific *Angptl4*-deficient mice, administration of *Angptl4* ASO resulted in decreased plasma TAGs, TC, HDL-C, and glucose levels (Figure 9, C and D). These findings were further confirmed by FPLC analysis (Supplemental Figure 8B). Similar to *Hmut* mice fed a CD, mice treated with *Angptl4* ASO also showed elevated HL and LPL activity without changes in body weight (Supplemental Figure 8, C–E).

To further determine whether therapeutic inhibition of *Angptl4* expression in the liver attenuates HFD-induced obesity and IR, mice were fed a HFD for 4 weeks, followed by administration of *Angptl4* ASO for 6 weeks along with HFD feeding (Figure 9E). *Angptl4* ASO treatment significantly protected against body weight gain and increase in fat mass in response to HFD feeding (Figure 9F). In addition, *Angptl4* inhibition resulted in decreased circulating TAGs compared with that in Ctrl ASO mice (Figure 9G and Supplemental Figure 8F). Plasma TC levels were slightly decreased in *AngptL4* ASO–treated mice, and HDL-C levels were similar in both groups of mice (Figure 9G and Supplemental Figure 8F). Moreover, we observed a significant improvement in glucose tolerance and insulin sensitivity in mice administered *Angptl4* ASO as compared with Ctrl ASO (Figure 9, H and I).

Since global *Angptl4* deficiency in mice leads to severe systemic metabolic and inflammatory complications when mice are fed for approximately 10 weeks on an HFD diet (26), we next assessed whether hepatocyte-specific inhibition of *Angptl4* using *Angptl4* ASO improves whole-body metabolic homeostasis without causing any deleterious effects. In contrast to complete loss of *Angptl4*, *Angptl4* ASO therapy does not influence gut inflammation, chylous ascites, MLN inflammation (presence of Touton giant cells and *Cxcl1*, *Ptgs2*, and *Ccr1* expression), or circulating leukocyte levels (Figure 9J and Supplemental Figure 9, A–D). These data indicate that the reduction in body weight of *Angptl4* ASO–treated mice (Supplemental Figure 9E) was not due to a reduction of food intake (Supplemental Figure 9F) or inflammation of the gut or MLN. We also found a significant reduction in the liver weight and hepatic TAG levels in mice treated with *Angptl4* ASO (Supplemental Figure 9, G and H). Additionally, *Angptl4* ASO–treated mice were protected against HFD-induced liver damage, as evidenced by lower plasma levels of hepatic enzymes alanine aminotransferase (ALT) and aspartate aminotransferase (AST) as well as reduced circulating liver-derived acute-phase protein SAA (Figure 9K and Supplemental Figure 9I). Together, these data indicate that specific silencing of *Angptl4* in the liver using GalNac-conjugated ASOs recapitulates the beneficial effects observed in *Hmut* mice under both physiological and pathological conditions. Most importantly, hepatic ANGPTL4 silencing was able to restore metabolic function in animals that were already obese, suggesting that this therapeutic approach may provide a viable treatment option for obesity-related metabolic disorders, including T2D and CVD.

Inhibition of the expression of hepatocyte-derived Angptl4 increases energy expenditure. Mice with hepatocyte-specific loss of *Angptl4* are protected against diet-induced obesity. To elucidate how hepatocyte-specific expression inhibition of *Angptl4* improves whole-body energy metabolism under HFD-fed conditions (after 6-week treatment of *Angptl4* ASO during HFD feeding), we performed metabolic cage analyses. We observed an increase in oxygen consumption, CO_2 production, energy expenditure (EE), and locomotor activity in *Angptl4* ASO–treated mice compared with Ctrl ASO–treated mice during dark and light cycles (Figure 10, A–D, and Supplemental Figure 10A). However, food consumption and respiratory exchange ratio (RER) remained unchanged (Figure 10E and Supplemental Figure 10B). Similarly, gut lipid (energy) absorption was not different between the groups (Supplemental Figure 10C). Together, these findings suggest that hepatocyte-specific deficiency of *Angptl4* reduces diet-induced obesity, likely by increasing EE.

Discussion

Elevated circulating TAGs lead to elevated risk of cardiometabolic diseases, such as obesity, T2D, and CVD, which are associated with increased adiposity, fatty liver, and IR (21–23, 25, 54, 55). Human studies have shown a positive correlation between ANGPTL4 function and BMI, fat mass, glucose intolerance, IR, and circulating lipids (25, 56, 57). These observations implicate ANGPTL4 as a mediator and potential therapeutic target for treating dyslipidemia-associated diseases. However, the exact function of ANGPTL4 in regulating whole-body lipid and glucose metabolism has not been fully elucidated due to the lack of tissue-specific KO mouse models. This is especially relevant because severe systemic metabolic complications (i.e., ascites, MLN, and gut inflammation) confound the researcher's ability to investigate the beneficial functions of *Angptl4* in whole-body KO mice upon HFD/WD feeding (26, 31). Since ANGPTL4 is highly expressed in the liver and AT of both humans and mice, we generated *Angptl4*-deficient mouse models specific to these tissues. Our previous work demonstrated that Ad-KO mice exhibit improved plasma lipid profiles and insulin sensitivity, but no difference in body weight was observed between Ad-KO and WT mice during prolonged HFD feeding (32). Similar results were recently reported by the Davies laboratory (33). As the overall impact on systemic metabolism was not as profound as expected, we hypothesized that ANGPTL4 derived from another vital metabolic organ involved in lipid homeostasis might be responsible for the effects on whole-body lipid and glucose metabolism observed in human studies. Interestingly, the ablation of hepatic ANGPTL4 resulted in decreased body weight, plasma lipids (TAGs and TC), and hepatic steatosis as well as improved glucose tolerance and insulin sensitivity after 16 weeks of HFD feeding. The effects observed in *Hmut* mice were more pronounced than those found in Ad-KO mice, indicating that the deficiency of ANGPTL4 in hepatocytes has major consequences on systemic lipid and glucose metabolism.

Since *Hmut* mice were generated via removal of exons 4–6, it is possible that truncated protein might still be produced. However, truncated protein might not be functional, as we observed a marked increase in HL and LPL activity both in the liver (primary hepatocytes) and post-heparin plasma in the *Hmut* mice. In agreement with this observation, the Kersten group has recently reported that *Angptl4* hypomorph mice (same mouse model as used in this study) have circulating TAG levels similar to those of the global *Angptl4*-deficient mice (58), suggesting that the ANGPTL4 truncated isoform does not affect LPL function. Moreover, Davies and colleagues have shown that the overexpression of an *Angptl4* construct similar

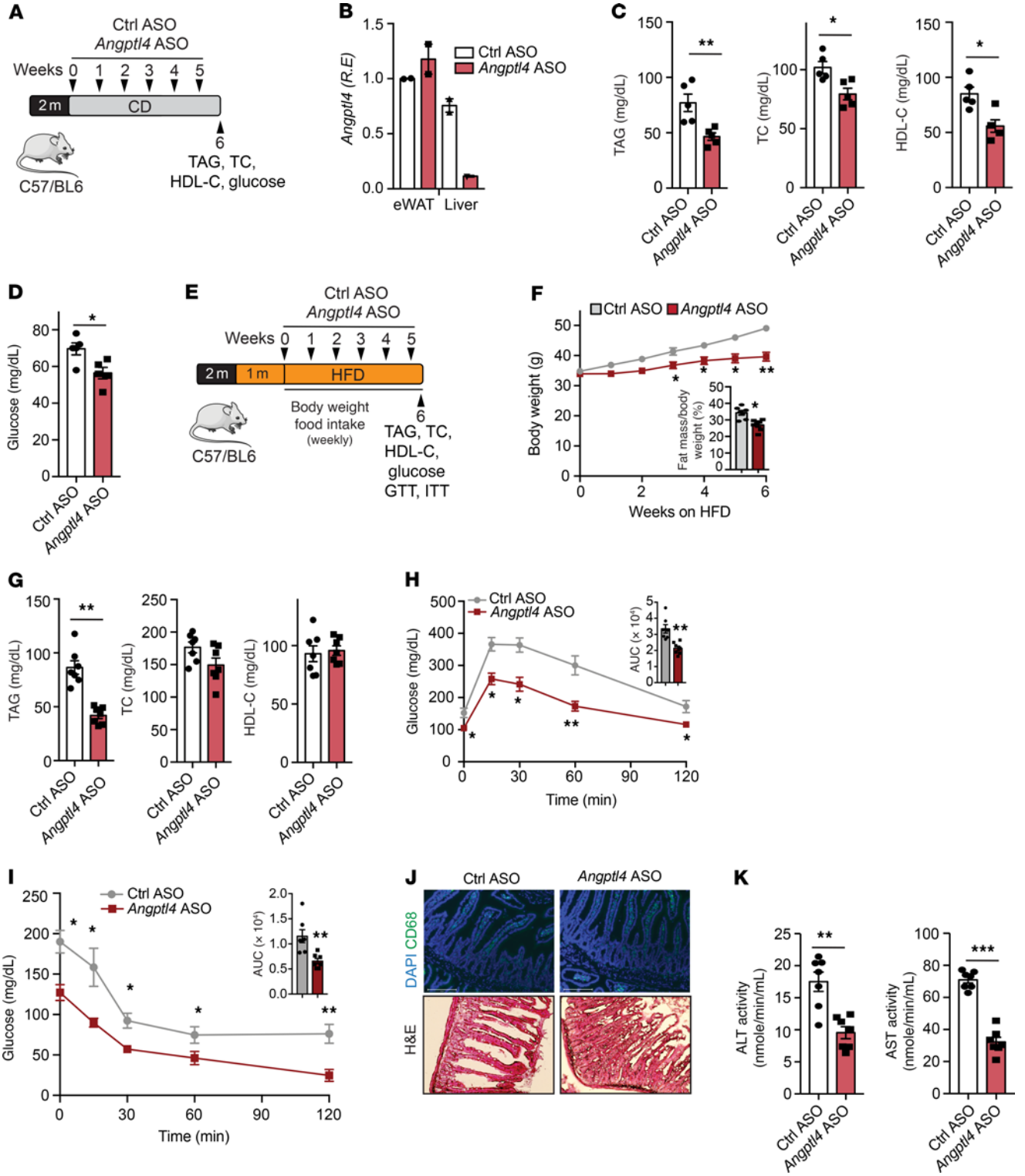

Figure 9. GalNac-conjugated ANGPTL4 ASO treatment improves whole-body metabolism under physiological and pathophysiological conditions. (**A**) Schematic presentation of the experimental design of GalNac-conjugated ANGPTL4 ASO (ANGPTL4 ASO) treatment of CD-fed mice. (**B**) *Angptl4* expression in eWAT and liver. (**C**) Plasma TAG, TC, and HDL-C from overnight-fasted 6-week *Angptl4* ASO or Ctrl ASO–treated WT mice. (**D**) Fasting blood glucose. (**E**) Strategy for treatment of GalNac-conjugated ANGPTL4 ASO in fat-induced obese mice. HFD-fed mice were treated with *Angptl4*-ASO or Ctrl ASO for 6 weeks. (**F**) Body weight: number of weeks on an HFD diet is indicated (treatment was started at week 5 of HFD feeding). Inset represents fat mass measured by Echo-MRI. (**G**) Plasma TAG, TC, and HDL-C from overnight-fasted 6 -week ANGPTL4 ASO– or Ctrl ASO–treated HFD-fed WT mice. (**H** and **I**) Intraperitoneal glucose tolerance test and intraperitoneal insulin tolerance test in 6-week ANGPTL4 ASO– or Ctrl ASO–injected mice fed an HFD. Inset represents AUC. (**J**) Representative images of small intestine cross sections of HFD-fed mice from 10-week treatment of *Angptl4* ASO or Ctrl ASO, stained with macrophage marker CD68 and H&E. Original magnification, ×20. (**K**) Activity of plasma ALT and AST after 10-week treatment of ANGPTL4 ASO or Ctrl ASO in HFD-induced obese mice. All data are represented as mean ± SEM. $^*P < 0.05$; $^{**}P < 0.01$; $^{***}P < 0.001$, comparing *Angptl4* ASO– with Ctrl ASO–treated mice using unpaired *t* test.

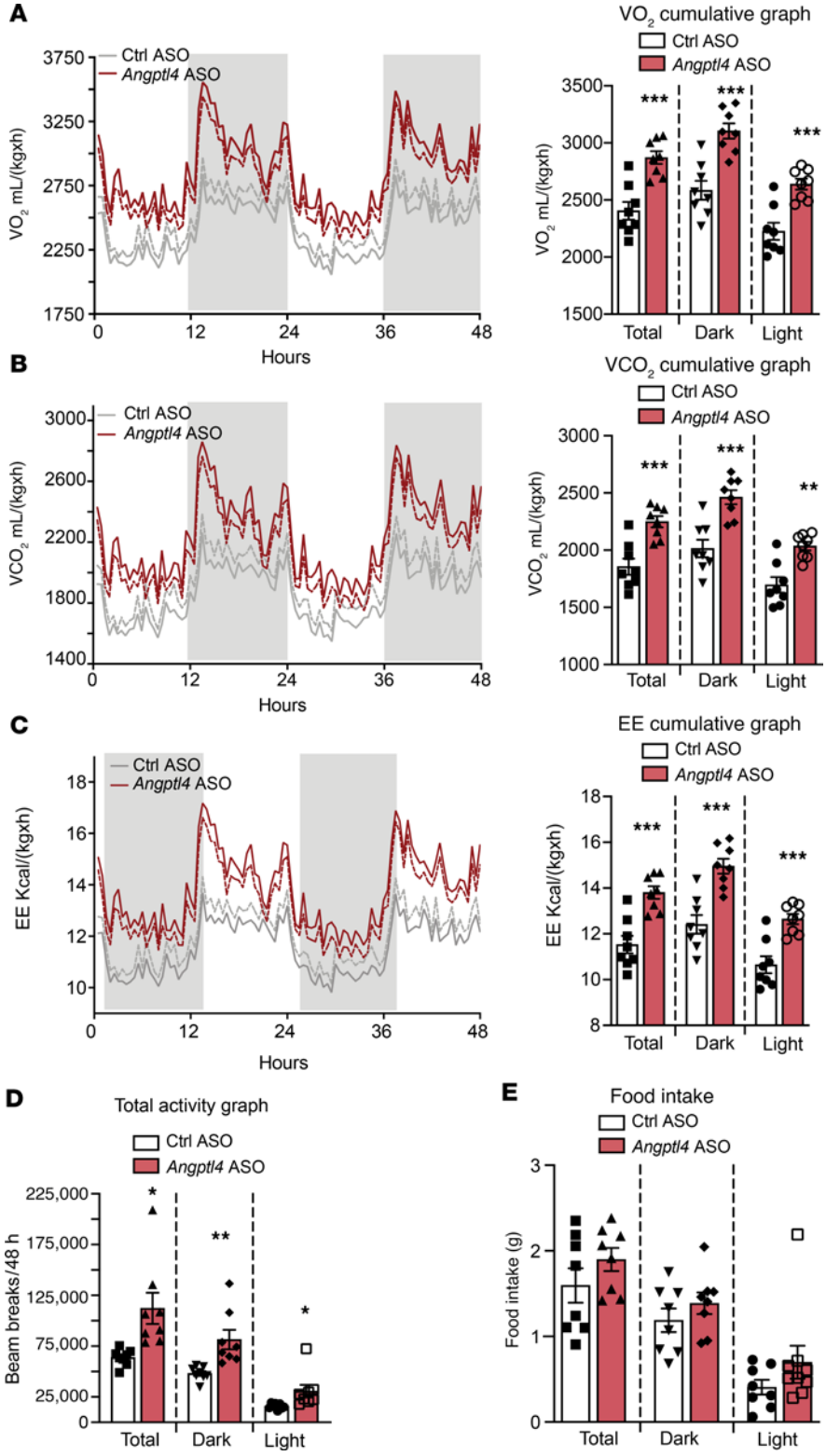

Figure 10. Suppression of hepatocyte *Angptl4* by GalNac-conjugated *Angptl4* ASO increases EE without influencing food intake. (**A**–**E**) Metabolic analysis of *Angptl4* ASO– and Ctrl ASO–treated HFD-fed mice over a 48-hour period. (**A**) Oxygen consumption. Right panel shows cumulative graph of O_2 consumption. (**B**) Carbon dioxide production. Cumulative graph on the right. (**C**) EE. Right section indicates cumulative graph. (**D**) Total activity. (**E**) Food consumption. All data are represented as mean ± SEM. $^*P < 0.05$; $^{**}P < 0.01$; $^{***}P < 0.001$, comparing *Angptl4* ASO– with Ctrl ASO–treated mice using an unpaired *t* test.

to the one used to develop our mouse model does not affect LPL activity (33). Together, these studies demonstrate that the potential truncated ANGPTL4 protein generated from this transcript is not functional and does not influence LPL activity in mice.

The improved circulating lipids in hepatocyte-specific *Angptl4* mutant mice was accompanied by accelerated TRL-remnant catabolism. We observed increased plasma TAG clearance and enhanced HL activity in *Hmut* mice. To confirm that ANGPTL4 regulates HL activity, we silenced HL in *Hmut* mice using siRNA and showed a reversal of the plasma lipid levels, indicating that ability of ANGPTL4 to decrease circulating TAG levels is mediated via HL-dependent TAG lipolysis in our model. These results are in line with a previous report by Lichtenstein and colleagues showing the suppression of postheparin HL activity in AT-specific overexpressing *Angptl4* mice (12). In contrast, other studies have shown that *Angptl4*-KO mice and liver-specific overexpression of *Angptl4* did not influence HL activity (28, 59). The reason for the discrepancy among these studies is unclear, but may be related to the differences in the mouse models used (magnitude of ANGPTL4 expression and overexpression of mouse *Angptl4* versus human *ANGPTL4*) and the sensitivity of the assay used for measuring plasma HL activity. Increased LPL activity in hepatocytes might also contribute to the reduced circulating TAGs due to decreased levels of VLDL, consistent with existing data from previous studies (12). Nevertheless, our data suggest that much of the systemic changes in lipid homeostasis in the absence of functional hepatic ANGPTL4 may be mediated by increased HL activity.

In addition to acting as a lipolytic enzyme, HL facilitates the uptake of chylomicrons and VLDL remnants by hepatocyte cell-surface receptors, thus contributing to the lowering of circulating lipids (60, 61). Comparison of FPLC plasma lipoprotein cholesterol profiles (IDL/LDL-fraction) in atherogenic mice further indicates that the protective impact of hepatic depletion of ANGPTL4 involves the contribution of elevated HL activity. Increased HL activity could facilitate the uptake of TRL remnants in hepatocytes to prevent the accumulation of atherogenic lipoproteins in atherosclerotic plaques (62). As such, genetic ablation of ANGPTL4 in hepatocytes markedly reduces circulating proatherogenic lipoproteins and attenuates the progression of atherosclerosis.

We also noticed that the depletion of hepatic ANGPTL4 leads to AMPK-mediated suppression of HMGCR expression and activity. Therefore, we believe that the suppressed activity of HMGCR in *Hmut* mice might contribute to reduced atherogenic lipoproteins and cholesterol in the plasma. These data suggest that hepatic ANGPTL4 may have a unique role in regulating both HL and HMGCR activity during the progression of atherosclerosis.

In contrast to our prior work in adipose-deficient *Angptl4* mice (32), we found that loss of hepatic ANGPTL4 protects against body weight gain upon HFD/WD feeding, mainly by reducing visceral fat mass and liver weight, without affecting food intake. Metabolic analyses suggest that depletion of hepatic ANGPTL4 resulted in substantially higher EE without affecting food intake, which supports the reduction of fat mass for maintaining the balance of whole-body energy metabolism. Moreover, the reduction in fat mass and size of adipocytes in *Hmut* mice may be due in part to the accelerated hydrolysis of TRL remnants and increased FA uptake in the liver, leading to decreased circulating TAGs and reduced lipid storage in AT. The role of ANGPTL4 in mouse body weight regulation under both physiological and pathophysiological conditions has been controversial (13, 21, 28, 32). The reasons for these discrepancies are unknown, but may be due to the inactivation of different exons of the N-terminus of ANGPTL4 between KO models, different types of diet, and the magnitude of overexpression. Structure-function analysis of ANGPTL4 from various KO models through protein crystallography or Cryo-EM may eventually justify these discordant findings.

Despite increased lipid uptake in the liver, we found a marked reduction in the intrahepatic lipid accumulation in *Hmut* mice. We also observed a concomitant increase in the rate of FAO in the liver, suggesting that excess fat taken up by the liver is dissipated through enhanced β-oxidation via activation of AMPK upon *Angptl4* deletion. AMPK is known to increase FAO and suppress DNL by inhibiting ACC. Thus, heightened AMPK activity may be one of the mechanisms by which hepatic deletion of *Angptl4* improves metabolic function following HFD-induced obesity. This hypothesis is supported by recent studies on the overexpression of AMPK in the mouse liver (63, 64). Moreover, ANGPTL4 has been reported to regulate AMPK activity to modulate metabolic homeostasis (42). Data from these studies indicate that activation of AMPK in the liver decreases lipid deposition not only in the liver, but also in the AT. Thus, improvements in whole-body glucose homeostasis and insulin action in *Hmut* mice upon prolonged HFD feeding are likely downstream of the marked reduction in lipid accumulation in the liver and AT.

In the present study, we demonstrate a mechanism by which ANGPTL4 regulates lipid homeostasis via a mechanism involving the HL/ROS/AMPK axis (Figure 8I). This mechanism is supported by several lines of evidence. First, increased lipase-mediated lipid uptake causes a compensatory increase in AMPK-mediated FAO (46). It is well established that AMPK is critical to the adaptive response of FA metabolism (65–67). Activated AMPK upregulates β-oxidation of FA by inhibiting ACC. Dysregulation of AMPK signaling is associated with a diminished capacity of regulating FAO to FA availability, leading to lipid accumulation and IR. Our study shows a prominent role of AMPK in controlling FA metabolism in hepatocytes lacking ANGPTL4. In addition, previous studies suggest that elevated FA or lipid accumulation can activate AMPK via CD36-dependent activation of LKB1 and independent of the cellular energy state (65–67). Our data also indicate that suppression of HL expression in hepatocytes lacking *Angptl4* attenuates the lipid uptake that is correlated with decreased AMPK activation and ROS generation. These findings suggest that the HL-mediated increase in FA uptake in hepatocytes lacking *Angptl4* is required for adaptive activation of AMPK. However, persistent activation of AMPK is required to fully promote the beneficial metabolic effects observed with hepatocyte-specific loss of ANGPTL4. It is known that FAO promotes ROS generation, and ROS is a well-known regulator of AMPK. Thus, ROS seems to play a key role in continually activating AMPK in hepatocytes, facilitating sustained FAO. Moreover, our data indicate that suppression of ROS-mediated AMPK activation is sufficient to reverse the metabolic phenotype observed in *Hmut* mice. Our data demonstrate that FAO is a source of ROS in ANGPTL4-deficient cells and that elevated ROS is required for maintaining an AMPK-dependent high rate of FAO (Figure 8I). ROS at a physiological level plays a key role in cellular signaling as well as in the regulation of several metabolic pathways (68). Our data suggest that reducing ROS with the scavenger NAC not only suppressed activation of AMPK, but also reversed changes in hepatic lipid metabolism in *Hmut* mice. These observations suggest that ROS is a key mediator underlying the inverse relationship between AMPK and ANGPTL4.

In recent years, studies have shown that ANGPTL4 acts as a potent metabolic regulator and is strongly associated with various metabolic disorders. Attempts to inhibit ANGPTL4 using a neutralizing antibody in humanized mice and nonhuman primates were confounded by severe systemic metabolic abnormalities (22). Our data from *Hmut* mice support the hypothesis that hepatocyte-specific suppression of *Angptl4* might have therapeutic potential in metabolic diseases. Therefore, we evaluated whether therapeutic inhibition of *Angptl4* expression in the liver recapitulates the beneficial metabolic phenotype afforded by genetic depletion of ANGPL4 in hepatocytes. Interestingly, *Angptl4* ASO–treated mice were ameliorated from HFD-induced obesity and had improved circulating TAGs, glucose tolerance, and insulin sensitivity. Conclusively, this study reveals that *Angptl4* ASO–mediated inhibition of hepatic *Angptl4* consistently replicates most aspects of the obesity-resistant phenotype observed in *Hmut* mice. Most importantly, mice treated with *Angptl4* ASO did not exhibit any of the systemic metabolic abnormalities observed in previous studies. Thus, this study provides a strong rationale for following the development of liver-specific ANGPTL4 therapeutic agents for treatment of cardiometabolic diseases.

Limitations. While the findings of this study, along with our prior work, have considerably improved our understanding of how ANGPTL4 in vital metabolic organs affects the ability to maintain metabolic homeostasis, there are still important questions and caveats that will need to be addressed in the future. Most importantly, ANGPTL4 is a secreted protein, and our current work has been unable to determine how the deficiency in the liver or AT precisely influences circulating levels of ANGPTL4 and what impact this may have on lipid metabolism in other tissues. To explore this further, a specific and reliable antibody against mouse ANGPTL4 needs to be generated to measure serum ANGPTL4 levels. In addition, we used a pharmacological inhibitor of AMPK, CompC, which might have off-target effects. Therefore, a genetic approach to silencing AMPK in the liver would be a useful secondary approach. Finally, in response to the loss of function of ANGPTL4 in hepatocytes, elevated HL

activity was associated with decreased plasma HDL-C under physiological conditions. However, this relationship was not apparent in pathophysiological situations, such as obesity and diabetes; thus, further mechanistic investigation is needed to elucidate the relationship between HL and HDL-C under lipid overload conditions.

Methods

Detailed information on experimental procedures and reagents is provided in Supplemental Methods.

Animal studies

Generation of hepatocyte-specific Angptl4-deficient mice. Mice bearing a loxP-flanked *Angptl4* allele (*ANGPTL4*$^{loxP/loxP}$ mice) were generated as described previously (32). Hepatocyte-specific *Angptl4*-deficient mice (Albumin-Cre; *Angptl4*$^{loxP/loxP}$, *Hmut*) were generated by breeding albumin-Cre; *Angptl4*$^{loxP/+}$ mice with *Angptl4*$^{loxP/+}$ mice. All mouse strains were in the BL6 genetic background. *Hmut* mice were verified recombination within the *Angptl4* gene in the liver by PCR using Cre primers and primers flanking the 5′ homology arm of the *Angptl4* gene and LoxP sites from the tail-extracted DNA. All experimental mice were housed in a barrier animal facility with a constant temperature and humidity on a 12-hour dark/12-hour light cycle, and water and food were provided ad libitum. All mice (n = 3–5 per cage) were fed with a standard CD for 8 weeks and afterwards switched to an HFD (60% calories from fat; Research Diets D12492) for 1 to 16 weeks. To assess whether ANGPTL4 regulates plasma lipid levels through an HL-mediated pathway, Hmut mice were injected with locked nucleic acid–conjugated (LNA-conjugated) siRNA against HL through a retro-orbital route at a dose of 20 mg/kg twice a week for 2 weeks. For atherosclerosis studies, mice (8 weeks old; n = 3-5 per cage) were administered a single retro-orbital injection of recombinant adeno-associated virus (AAV) (containing 1.0×10^{11} genome copies) encoding PCSK9 (AAV8.ApoEHCR-hAAT.D377Y-mPCK9.bGH) to induce hyperlipidemia (32). Two weeks after injection, atherosclerosis was induced by feeding the mice with a high-cholesterol WD containing 1.25% cholesterol (D12108, Research Diets). Body weight and food intake were measured every week for HFD- and WD-fed mice.

For liver-specific *Angptl4* ASO studies, mice at 10 weeks of age were injected with Ctrl ASO or GalNac conjugate *Angptl4* ASO (*Angptl4* ASO) (the combination of 2 ASOs) through retro-orbital route at a dose of 25 mg/kg/wk for 6 weeks. ASO sequences used in this study were as follows: *Angptl4* ASO: (a) 5′-AGCTGTAGCAGCCCGT-3′; (b) 5′-ATATGACTGAGTCCGC-3′ and Ctrl ASO 5′-GGCCAATACGCCGTCA-3′. ASOs were dissolved in PBS for the mouse experiments. During the GalNac-conjugated *Angptl4* ASO treatment, mice were fed with CD. To assess the therapeutic effect of GalN-ASO in obese mice, mice were fed an HFD for 4 weeks and were treated with GalNac–Ctrl ASO or GalNac–*Angptl4* ASO (25 mg/kg) by retro-orbital injections weekly for the 10 weeks.

Statistics

The mouse sample size for each study was based on literature documentation of similar well-characterized experiments. The number of mice used in each study is listed in the figure legends. In vitro experiments were regularly repeated at least 3 times unless otherwise noted. No inclusion or exclusion criteria were used, and studies were not blinded to investigators or formally randomized. Data are expressed as average ± SEM. Statistical differences were measured using an unpaired 2-sided Student's t test or 1-way or 2-way ANOVA with Bonferroni's correction for multiple comparisons. Normality was tested using the Kolmogorov-Smirnov test. A nonparametric test (Mann-Whitney U test) was used when the data did not pass the normality test. $P \leq 0.05$ was considered statistically significant. Data analysis was performed using GraphPad Prism software, version 7.

Study approval

Animal experiments were conducted under the ethical guidelines of and protocols were approved by the IACUC at Yale University School of Medicine (animal protocol 2019-11577).

Author contributions

AKS, BC, YS, and CFH conceived and designed the study and wrote the manuscript. AKS, BC, ACD, XZ, BA, JS, KMC, LV, and NR performed experiments and analyzed data. NLP, KMC, and TLH analyzed data and edited the manuscript. RGL provide the antisense oligonucleotides used to inhibit the expression of hepatic ANGPTL4.

Acknowledgments

This work was supported at least in part by grants from the NIH (R35HL135820 to CFH and 5F32DK10348902 to NLP), the American Heart Association (16EIA27550005 to CFH, 20TPA35490202 to YS and 17SDG33110002 to NR), and the American Diabetes Association (1-16-PMF-002 to ACD).

Address correspondence to: Carlos Fernández-Hernando or Yajaira Suárez, 10 Amistad Street, Room 337c, New Haven, Connecticut 06520, USA. Phone: 203.737.4615; Email: carlos.fernandez@yale.edu (CFH). Phone: 203.737.8858; Email: yajaira.suarez@yale.edu (YS).

1. Bechmann LP, et al. The interaction of hepatic lipid and glucose metabolism in liver diseases. *J Hepatol*. 2012;56(4):952–964.
2. Petersen MC, et al. Regulation of hepatic glucose metabolism in health and disease. *Nat Rev Endocrinol*. 2017;13(10):572–587.
3. Fabbrini E, et al. Obesity and nonalcoholic fatty liver disease: biochemical, metabolic, and clinical implications. *Hepatology*. 2010;51(2):679–689.
4. Gancheva S, et al. Interorgan metabolic crosstalk in human insulin resistance. *Physiol Rev*. 2018;98(3):1371–1415.
5. Hodson L. Hepatic fatty acid synthesis and partitioning: the effect of metabolic and nutritional state. *Proc Nutr Soc*. 2019;78(1):126–134.
6. Cusi K. Role of obesity and lipotoxicity in the development of nonalcoholic steatohepatitis: pathophysiology and clinical implications. *Gastroenterology*. 2012;142(4):711–725.
7. Nakajima K, et al. Postprandial lipoprotein metabolism: VLDL vs chylomicrons. *Clin Chim Acta*. 2011;412(15–16):1306–1318.
8. Cohen JC, et al. Human fatty liver disease: old questions and new insights. *Science*. 2011;332(6037):1519–1523.
9. Farese RV Jr., et al. The problem of establishing relationships between hepatic steatosis and hepatic insulin resistance. *Cell Metab*. 2012;15(5):570–573.
10. Petersen KF, et al. Reversal of nonalcoholic hepatic steatosis, hepatic insulin resistance, and hyperglycemia by moderate weight reduction in patients with type 2 diabetes. *Diabetes*. 2005;54(3):603–608.
11. Browning JD, Horton JD. Molecular mediators of hepatic steatosis and liver injury. *J Clin Invest*. 2004;114(2):147–152.
12. Lichtenstein L, et al. Angptl4 upregulates cholesterol synthesis in liver via inhibition of LPL- and HL-dependent hepatic cholesterol uptake. *Arterioscler*

Thromb Vasc Biol. 2007;27(11):2420–2427.
13. Mandard S, et al. The fasting-induced adipose factor/angiopoietin-like protein 4 is physically associated with lipoproteins and governs plasma lipid levels and adiposity. *J Biol Chem*. 2006;281(2):934–944.
14. Kersten S, et al. Characterization of the fasting-induced adipose factor FIAF, a novel peroxisome proliferator-activated receptor target gene. *J Biol Chem*. 2000;275(37):28488–28493.
15. Zhu P, et al. Angiopoietin-like 4: a decade of research. *Biosci Rep*. 2012;32(3):211–219.
16. Kristensen KK, et al. Unfolding of monomeric lipoprotein lipase by ANGPTL4: insight into the regulation of plasma triglyceride metabolism. *Proc Natl Acad Sci U S A*. 2020;117(8):4337–4346.
17. Aryal B, et al. ANGPTL4 in metabolic and cardiovascular disease. *Trends Mol Med*. 2019;25(8):723–734.
18. Kersten S. New insights into angiopoietin-like proteins in lipid metabolism and cardiovascular disease risk. *Curr Opin Lipidol*. 2019;30(3):205–211.
19. Dijk W, Kersten S. Regulation of lipoprotein lipase by Angptl4. *Trends Endocrinol Metab*. 2014;25(3):146–155.
20. Desai U, et al. Lipid-lowering effects of anti-angiopoietin-like 4 antibody recapitulate the lipid phenotype found in angiopoietin-like 4 knockout mice. *Proc Natl Acad Sci U S A*. 2007;104(28):11766–11771.
21. Gusarova V, et al. Genetic inactivation of ANGPTL4 improves glucose homeostasis and is associated with reduced risk of diabetes. *Nat Commun*. 2018;9(1):2252.
22. Dewey FE, et al. Variants in ANGPTL4 and the risk of coronary artery disease. *N Engl J Med*. 2016;375(23):2305–2306.
23. Klarin D, et al. Genetics of blood lipids among ~300,000 multi-ethnic participants of the Million Veteran Program. *Nat Genet*. 2018;50(11):1514–1523.
24. Liu DJ, et al. Exome-wide association study of plasma lipids in >300,000 individuals. *Nat Genet*. 2017;49(12):1758–1766.
25. Barja-Fernandez S, et al. Plasma ANGPTL-4 is associated with obesity and glucose tolerance: cross-sectional and longitudinal findings. *Mol Nutr Food Res*. 2018;62(10):e1800060.
26. Lichtenstein L, et al. Angptl4 protects against severe proinflammatory effects of saturated fat by inhibiting fatty acid uptake into mesenteric lymph node macrophages. *Cell Metab*. 2010;12(6):580–592.
27. Janssen AWF, et al. Loss of angiopoietin-like 4 (ANGPTL4) in mice with diet-induced obesity uncouples visceral obesity from glucose intolerance partly via the gut microbiota. *Diabetologia*. 2018;61(6):1447–1458.
28. Koster A, et al. Transgenic angiopoietin-like (angptl)4 overexpression and targeted disruption of angptl4 and angptl3: regulation of triglyceride metabolism. *Endocrinology*. 2005;146(11):4943–4950.
29. Xu A, et al. Angiopoietin-like protein 4 decreases blood glucose and improves glucose tolerance but induces hyperlipidemia and hepatic steatosis in mice. *Proc Natl Acad Sci U S A*. 2005;102(17):6086–6091.
30. Wang Y, et al. Angiopoietin-like protein 4 improves glucose tolerance and insulin resistance but induces liver steatosis in high-fat-diet mice. *Mol Med Rep*. 2016;14(4):3293–3300.
31. Aryal B, et al. ANGPTL4 deficiency in haematopoietic cells promotes monocyte expansion and atherosclerosis progression. *Nat Commun*. 2016;7:12313.
32. Aryal B, et al. Absence of ANGPTL4 in adipose tissue improves glucose tolerance and attenuates atherogenesis. *JCI Insight*. 2018;3(6):97918.
33. Spitler KM, et al. Regulation of plasma triglyceride partitioning by adipose-derived ANGPTL4 in mice. *Sci Rep*. 2021;11(1):7873.
34. Boren J, et al. Ectopic lipid storage and insulin resistance: a harmful relationship. *J Intern Med*. 2013;274(1):25–40.
35. Petersen MC, Shulman GI. Mechanisms of insulin action and insulin resistance. *Physiol Rev*. 2018;98(4):2133–2223.
36. Stender S, et al. Adiposity amplifies the genetic risk of fatty liver disease conferred by multiple loci. *Nat Genet*. 2017;49(6):842–847.
37. Sarwar R, et al. Obesity and nonalcoholic fatty liver disease: current perspectives. *Diabetes Metab Syndr Obes*. 2018;11:533–542.
38. Moshage H. Cytokines and the hepatic acute phase response. *J Pathol*. 1997;181(3):257–266.
39. Softic S, et al. Role of dietary fructose and hepatic de novo lipogenesis in fatty liver disease. *Dig Dis Sci*. 2016;61(5):1282–1293.
40. Sinha RA, et al. Direct effects of thyroid hormones on hepatic lipid metabolism. *Nat Rev Endocrinol*. 2018;14(5):259–269.
41. Samovski D, et al. Regulation of AMPK activation by CD36 links fatty acid uptake to β-oxidation. *Diabetes*. 2015;64(2):353–359.
42. Kim HK, et al. Hypothalamic Angptl4/Fiaf is a novel regulator of food intake and body weight. *Diabetes*. 2010;59(11):2772–2780.
43. Steinberg GR, Carling D. AMP-activated protein kinase: the current landscape for drug development. *Nat Rev Drug Discov*. 2019;18(7):527–551.
44. Liemburg-Apers DC, et al. Interactions between mitochondrial reactive oxygen species and cellular glucose metabolism. *Arch Toxicol*. 2015;89(8):1209–1226.
45. Shafique E, et al. Oxidative stress improves coronary endothelial function through activation of the pro-survival kinase AMPK. *Aging (Albany NY)*. 2013;5(7):515–530.
46. Schonfeld P, Wojtczak L. Fatty acids as modulators of the cellular production of reactive oxygen species. *Free Radic Biol Med*. 2008;45(3):231–241.
47. Pike LS, et al. Inhibition of fatty acid oxidation by etomoxir impairs NADPH production and increases reactive oxygen species resulting in ATP depletion and cell death in human glioblastoma cells. *Biochim Biophys Acta*. 2011;1807(6):726–734.
48. Dalle Pezze P, et al. A systems study reveals concurrent activation of AMPK and mTOR by amino acids. *Nat Commun*. 2016;7:13254.
49. Li Y, et al. AMPK phosphorylates and inhibits SREBP activity to attenuate hepatic steatosis and atherosclerosis in diet-induced insulin-resistant mice. *Cell Metab*. 2011;13(4):376–388.
50. Bhandary B, et al. An involvement of oxidative stress in endoplasmic reticulum stress and its associated diseases. *Int J Mol Sci*. 2012;14(1):434–456.
51. Cnop M, et al. Endoplasmic reticulum stress, obesity and diabetes. *Trends Mol Med*. 2012;18(1):59–68.
52. Hummasti S, Hotamisligil GS. Endoplasmic reticulum stress and inflammation in obesity and diabetes. *Circ Res*. 2010;107(5):579–591.
53. Prakash TP, et al. Targeted delivery of antisense oligonucleotides to hepatocytes using triantennary N-acetyl galactosamine improves potency 10-fold in mice. *Nucleic Acids Res*. 2014;42(13):8796–8807.
54. Mooradian AD. Dyslipidemia in type 2 diabetes mellitus. *Nat Clin Pract Endocrinol Metab*. 2009;5(3):150–159.
55. Do R, et al. Common variants associated with plasma triglycerides and risk for coronary artery disease. *Nat Genet*. 2013;45(11):1345–1352.
56. Bailetti D, et al. ANGPTL4 gene E40K variation protects against obesity-associated dyslipidemia in participants with obesity. *Obes Sci Pract*. 2019;5(1):83–90.
57. Barja-Fernandez S, et al. ANGPTL-4 is associated with obesity and lipid profile in children and adolescents. *Nutrients*. 2019;11(6):E1340.
58. Oteng AB, et al. Characterization of ANGPTL4 function in macrophages and adipocytes using *Angptl4*-knockout and *Angptl4*-hypomorphic mice. *J Lipid Res*. 2019;60(10):1741–1754.
59. Gutgsell AR, et al. Mapping the sites of the lipoprotein lipase (LPL)-angiopoietin-like protein 4 (ANGPTL4) interaction provides mechanistic insight into LPL inhibition. *J Biol Chem*. 2019;294(8):2678–2689.
60. Havel RJ, Hamilton RL. Hepatic catabolism of remnant lipoproteins: where the action is. *Arterioscler Thromb Vasc Biol*. 2004;24(2):213–215.
61. Brasaemle DL, et al. Hepatic lipase treatment of chylomicron remnants increases exposure of apolipoprotein E. *J Lipid Res*. 1993;34(3):455–465.
62. Toth PP. Triglyceride-rich lipoproteins as a causal factor for cardiovascular disease. *Vasc Health Risk Manag*. 2016;12:171–183.
63. Garcia D, et al. Genetic liver-specific AMPK activation protects against diet-induced obesity and NAFLD. *Cell Rep*. 2019;26(1):192–208.
64. Foretz M, et al. AMPK activation reduces hepatic lipid content by increasing fat oxidation in vivo. *Int J Mol Sci*. 2018;19(9):E2826.
65. Watt MJ, et al. Fatty acids stimulate AMP-activated protein kinase and enhance fatty acid oxidation in L6 myotubes. *J Physiol*. 2006;574(Pt 1):139–147.
66. Clark H, et al. Covalent activation of heart AMP-activated protein kinase in response to physiological concentrations of long-chain fatty acids. *Eur J Biochem*. 2004;271(11):2215–2224.
67. Hickson-Bick DL, et al. Palmitate-mediated alterations in the fatty acid metabolism of rat neonatal cardiac myocytes. *J Mol Cell Cardiol*. 2000;32(3):511–519.
68. Schieber M, Chandel NS. ROS function in redox signaling and oxidative stress. *Curr Biol*. 2014;24(10):R453–R462.